Geophysical Journal International

Geophys. J. Int. (2016) **204,** 180–199
GJI Geodynamics and tectonics

doi: 10.1093/gji/ggv443

New constraints on extensional tectonics and seismic hazard in northern Attica, Greece: the case of the Milesi Fault

Christoph Grützner,[1,*] Sascha Schneiderwind,[1] Ioannis Papanikolaou,[2,3] Georgios Deligiannakis,[2] Aggelos Pallikarakis[2] and Klaus Reicherter[1]

[1]*Institute of Neotectonics and Natural Hazards, RWTH Aachen University, Lochnerstr.* 4–20, *D*-52064 *Aachen, Germany. E-mail: chg39@cam.ac.uk*
[2]*Laboratory Mineralogy - Geology, Agricultural University of Athens, Iera Odos* 75, *Athina* 118 55, *Greece*
[3]*UCL Hazard Research Centre, Department of Earth Sciences, University College London, WC* 1*E* 6*BT, London, United Kingdom*

Accepted 2015 October 12. Received 2015 September 23; in original form 2014 September 7

SUMMARY

Northern Attica in Greece is characterized by a set of north dipping, subparallel normal faults. These faults were considered to have low tectonic activity, based on historical earthquake reports, instrumental seismicity and slip rate estimates. This study presents new data for one of these faults, the Milesi Fault. We run GIS based geomorphological analyses on fault offset distribution, field mapping of postglacial fault scarps and ground penetrating radar profiling to image hangingwall deformation. The first palaeoseismological trenching in this part of Greece allowed obtaining direct data on slip rates and palaeoearthquakes. The trenching revealed downthrown and buried palaeosols, which were dated by radiocarbon. The results of our investigations show that the slip rates are higher than previously thought and that at least four palaeoearthquakes with magnitudes of around *M*6.2 occurred during the last 4000–6000 yr. We calculate an average recurrence interval of 1000–1500 yr and a maximum throw rate of ∼0.4–0.45 mm a^{-1}. Based on the new geological earthquake data we developed a seismic hazard scenario, which also incorporates geological site effects. Intensities up to IX must be expected for Northern Attica and the southeastern part of Evia. Earthquake environmental effects like liquefaction and mass movements are also likely to occur. This scenario is in contrast to the official Greek seismic hazard zonation that is based on historical records and assigns different hazard zones for municipalities that will experience the same intensity by earthquakes on the Milesi Fault. We show that the seismic hazard is likely underestimated in our study area and emphasize the need to incorporate geological information in such assessments.

Key words: Palaeoseismology; Seismicity and tectonics; Continental tectonics: extensional; Neotectonics.

1 INTRODUCTION

During the last decades it became evident that faults with a relatively low slip rate might significantly contribute to the seismic hazard of a certain area. Large fault systems with high slip rates, high magnitudes and short recurrence intervals are easily recognized in most cases. They yield a clear geomorphological expression and have likely ruptured during historical times. Much is known about the earthquake history of these major structures and, therefore, they are accounted for in seismic hazard assessments. Recently, several moderate earthquakes in Europe caused fatalities and significant damage. Their consequences were confined to relatively small areas, but the quakes 2009 in L'Aquila (M_w 6.3), 2011 in Lorca (M_w 5.1) and 2012 in the Emilia-Romagna region (M_w 5.8) made clear that smaller fault systems must be considered an underestimated threat (Grützner *et al*. 2013), especially in densely populated areas. Unfortunately, not much is known about the kind of faults that ruptured during these quakes. In most cases they slip rather slowly (often less than 1 mm a^{-1}) and their length is in the order of 10–20 km only. Such active faults with recurrence intervals of several ka and low slip rates are often much harder to be identified in the field due to a number of reasons: (1) The faults may not have produced any earthquake during the era of instrumental observations; (2) No earthquake might be found in historical reports and in archaeological sites; (3) Sedimentation and erosion can obscure hints for active faulting in the landscape, if their rates are higher than fault slip-rates; (4) The ruptures may not have reached the surface

*Now at: COMET; Bullard Laboratories, Department of Earth Sciences, University of Cambridge, Madingley Rise, Madingley Road, CB3 0EZ, Cambridge, United Kingdom.

and (5) The faults might be known but considered inactive for the above listed reasons.

Their contribution to seismic hazard is therefore easily overlooked or remains unclear. The identification of such faults and palaeoseismological investigations of capable seismic sources can be considered the only way to overcome these problems and to properly include these structures in seismic hazard assessments. The low slip per event and the geological setting of such faults pose a certain challenge to palaeoseismological studies.

In the Athens Metropolitan Area (AMA) in northern Attica (Greece) several faults with a geomorphological expression are known, but historical and instrumental seismicity is rather low and little direct information is available on the slip rates, recurrence intervals and maximum earthquake magnitude. Athens and its surroundings have been hit by damaging earthquakes repeatedly (Fig. 1), but no major devastating earthquakes can be found in the instrumental and historical records. Archaeoseismological data evidence that no major shaking occurred in Athens during the last 2300 yr (Ambraseys & Psycharis 2012). The few events that caused damage to the AMA were either strong, but distant quakes like the 1981 Gulf of Corinth earthquake series with magnitudes of up to M6.7, or local but moderate events such as the 1999 $M_s = 5.9$ close to Athens. A strong and damaging earthquake is reported for 1705, with its epicentre somewhere between the towns of Athens and Chalkida, but it cannot surely be ascribed to one of the mapped sources (Papanikolaou & Papanikolaou 2007). Ambraseys & Jackson (1997) conclude that it had significant local effects, but that it was not a large magnitude event. On 1874 March 18 an earthquake probably not exceeding M6 caused some minor damage in Eretria and Chalkida, north of our study area (Papazachos & Papazachou 1997). Another significant earthquake occurred in 1938 in Oropos, 30 km north of the capital. This event caused intense local damage (generating macroseismic intensity VIII and 18 fatalities), but did not affect Athens (*cf.* Ambraseys & Jackson 1990). Due to uncertainties in the epicentral location its seismic source is not clear. In 1999, a shallow moderate quake of magnitude M_s 5.9 caused 143 deaths and $3 billion of damage in Athens (Papadopoulos *et al*. 2000a). This quake came as a surprise since seismogenic sources in the AMA were unknown at that time or underestimated. No tectonically active structure was known to exist in the vicinity of the epicentre of the 1999 earthquake (Pavlides *et al*. 2002). However, this surprising event marked also a difference in how seismic hazard was perceived in the society and attention was drawn onto the hazard posed by small and local faults (e.g. Zygouri *et al*. 2013).

At least ten faults with a clear surface expression are known in the vicinity of the AMA (Fig. 1, Ganas *et al*. 2004, 2005;

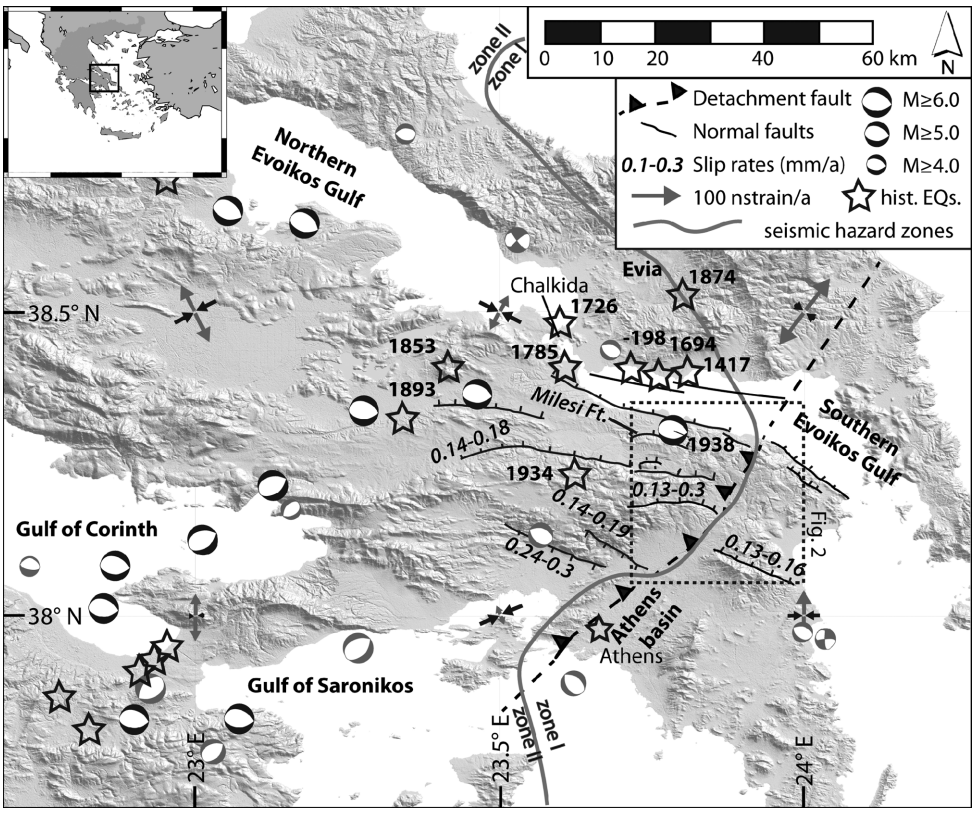

Figure 1. Active faults in Central Greece. Faults were compiled from Papanikolaou & Papanikolaou (2007), Papanikolaou *et al*. (1989) and own mapping. Note that only faults in the broader study area are indicated and not those of the Gulf of Corinth and Northern Evoikos Gulf systems. Seismic hazard zonation is from EAK (2003). Available moment tensor solutions from shallow quakes (<30 km) were collected from Ambraseys & Jackson (1990) and from Papadimitriou & Karakostas (2003) (black beach balls), grey beach balls come from the CMT and NOA catalogues (Dziewonski *et al*. 1981; Ekström *et al*. 2012; NOA 2014). Only one significant instrumental earthquake occurred in the study area close to the Milesi Fault, the Oropos 1938 event. Historical earthquake data (stars) were compiled using the AHEAD database (AHEAD 2014), Ambraseys & Jackson (1998), Papazachos & Papazachou (1997) and Papazachos *et al*. (2000). More events are published in Papazachos *et al*. (2000) but were not included here because they have relatively small magnitudes. The epicentre of the 1705 earthquake is not included, because its location is not well constrained (Ambraseys & Jackson 1997). It is only known that it occurred between the cities of Athens and Chalkida. The motion of the Aegean plate relative to Eurasia is about 30 mm a^{-1} towards the SW. Strain rates are from Hollenstein *et al*. (2008). Estimates on slip rates are from Ganas *et al*. (2005) and Papanikolaou & Papanikolaou (2007). This map is in Mercator Projection.

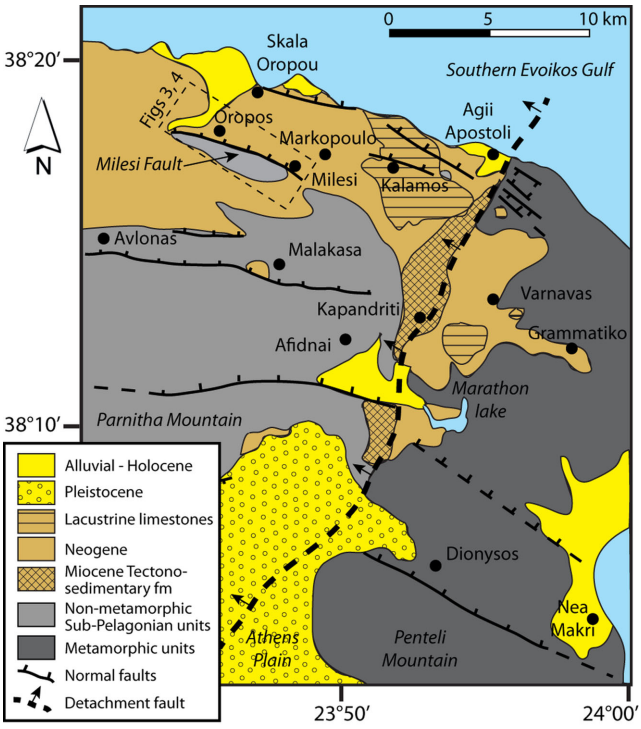

Figure 2. Geological setting and regional tectonics of the study area. Normal faults are straight lines (mapped and after Papanikolaou & Papanikolaou 2007), inferred faults are dashed thin lines; the detachment fault is marked with a thick dashed line, arrows indicate dip direction (after Papanikolaou & Papanikolaou 2007). Offshore faults are not drawn on this map. Normal faults identified in offshore seismic surveys are north-dipping, strike parallel to the coast line and also follow the coastline's change of direction east of Agii Apostoli (Papanikolaou *et al*. 1988a,b; Perissoratis & van Andel 1991; Smith 1994). The footwall of the Milesi Fault marks the northernmost outcrop of the Sub-Pelagonian Unit. Geology modified from Papanikolaou & Papanikolaou (2007).

Papanikolaou & Papanikolaou 2007), but precise information on earthquake history, slip rates, maximum magnitudes, fault segmentation, recurrence intervals and other data yet have to be gathered. The data will also be required for analysing the distribution of tectonic movements among the local and regional faults. The nearby Gulf of Corinth and the Evoikos Gulf are known to host significant amounts of extension, but it is not clear how deformation is distributed in the areas in between.

We investigated one fault to the north of Athens, the Milesi Fault (Figs 1 and 2). This structure is rather short (∼10 km) and might therefore represent the type of seismic source that caused the 1705 and 1938 earthquakes, with a magnitude in the order of *M*6.0–*M*6.2 and significant local consequences. Seismic events here could be significantly larger than the 1874 event or the 1999 earthquake that caused fatalities and damage in Athens. No recent, historical or pre-historical earthquake is known from this fault. Most palaeoseismological studies tend to focus on recently activated structures (e.g. Pantosti *et al*. 1996; Benedetti *et al*. 2003; Chatzipetros *et al*. 2005), which nevertheless are not expected to rupture again in the next few hundreds of years. The Milesi Fault could, if active, be at any stage of its seismic cycle.

Here, promising outcrops were found and fault scarps of most likely postglacial age are present. We performed geomorphological analyses based on a digital elevation model, geological mapping, geophysical investigations and palaeoseismological trenching in order to find out whether the Milesi Fault has to be considered active or not and in order to determine its slip rate, recurrence interval, last earthquake and maximum possible magnitude.

This paper provides evidence for morphogenic events during the Holocene [in the sense of Caputo (2005) and Caputo *et al*. (2008)], and new data on maximum magnitudes, slip rates and recurrence intervals. We use these data to estimate possible earthquake environmental effects in a typical earthquake scenario and we describe the hazard posed by the Milesi Fault. It is shown that the present seismic hazard zonation in the study area does not reflect the available geological knowledge. This paper reports on the first palaeoseismological study in Attica and demonstrates that palaeoseismological studies can successfully be performed on low slip rate normal faults which lack any earthquake record, even under the challenging conditions of low offset per event, stratigraphic constraints and the limitations due to the regional geological setting. We also introduce a new GIS-based approach to identify promising sites for on-fault investigations such as palaeoseismological trenching. This technique might help to identify sites where the faults' maximum slip is located.

2 GEOLOGICAL SETTING

In this section, we describe the local geology and the tectonic setting of the study area. We briefly summarize the knowledge on historical and instrumental seismicity. The last part of this section deals with the seismic hazard zonation and the setting of the study site.

A general issue with active faults in Greece (and also other regions like Italy) is that they are referred to with different names in the literature. The fault analysed in this study has been mentioned by Goldsworthy *et al*. (2002) as the Oropos Fault, named after the nearby small town of Oropos. Other studies, however, use the term *Oropos Fault* to describe the fault north of the one analysed in this paper, which runs through the town of Skala Oropou and may continue offshore (e.g. Papanikolaou *et al*. 1988a,b; Fig. 2). Naming the here investigated structure 'Oropos Fault' would inevitably add to this problem. We decided to use the term *Milesi Fault* after the town of Milesi which is located directly on the fault trace to avoid any confusion. Also, we do not use ambiguous names for other close-by faults in the study area, as there are similar problems with these, too. The Greek Database of Seismogenic Sources (GreDaSS; Caputo & Pavlides 2013) does not yet include sufficient information from our study area to solve this issue.

2.1 Geology of northern Attica

The geology of Central Greece is characterized by NNW–SSE orientated tectonic units that result from the complex stacking of mainly marine rocks during the closure of the Tethys. Ophiolites occur at various locations in between the marine nappes and tectonic windows are present (Papanikolaou 2009). The lithology includes non-metamorphic as well as metamorphic deep, intermediate and shallow marine sediments, flysch units and Neogene-recent basin deposits.

The geology of the AMA in Attica is divided in three major units: (1) metamorphic basement units; (2) non-metamorphic basement units and (3) postalpine sedimentary units (Jacobshagen 1986; Katsikatsos 2000). To the NE of Athens, metamorphic rocks occupy the area from Mt Penteli to the Evoikos Gulf. These Alpine units consist of massive Mesozoic marbles and locally overlying Tertiary phyllites (Papanikolaou & Papanikolaou 2007). Non-metamorphic mountain ranges to the north and northwest of Athens also formed

during the Alpine orogeny and consist of Sub-Pelagonian rocks. In between the two main basement units, clastic Miocene sediments are preserved, also referred to as tectonosedimentary formation (Papanikolaou & Papanikolaou 2007), overlain by a few hundred metres of Pliocene lacustrine limestones. These limestones also unconformably overlie the metamorphic basement in the east. Pleistocene and younger alluvium are present in depressions and along the coasts (Fig. 2).

The Alpine metamorphic units must have experienced a large amount of uplift in geologically short time, about 25 km. A large-scaled NNE–SSW running, W-dipping detachment is assumed to run from the Saronic Gulf in the SW through the Athens Basin to the Evoikos Gulf in the NE (Drakatos *et al*. 2005; Papanikolaou & Royden 2007; Krohe *et al*. 2010; Bradley 2012). Across this structure neotectonic fault orientation, recent microseismicity and regional strain do change (Papanikolaou & Lozios 1990; Foumelis *et al*. 2013). This structure called the Attica Detachment is also thought to be responsible for the formation of the Miocene tectonosedimentary debris flow formation in between the metamorphic and non-metamorphic rocks (Papanikolaou & Papanikolaou 2007). This structure must have been active from Late Miocene to Early Pliocene. The basal debris flow formation probably correlates with a similar formation exposed in the Kymi–Aliveri basin in Central Evia, where the same detachment is traced, and has an inferred Middle Miocene age (<13.5 Ma) based on radiometric dating of pyro-clastic ejecta interbedded with the underlying fluvial sequence (Bradley 2012).

2.2 Local tectonic setting and seismicity

Active faulting in the study area is controlled by the opening of the Evoikos and Corinth Gulfs in the broader frame of the Hellenic Subduction Zone and the westward motion of the Anatolian plate (McKenzie 1978; Taymaz *et al*. 1991). Jolivet *et al*. (2013) provide a detailed review of different views on Aegean tectonics. An extensional tectonic regime dominates the broader study area (Ambraseys & Jackson 1990, 1998) and led to the formation of the Evoikos Gulf Graben to the north and the Gulf of Corinth in the west. The formation of these rift zones is likely linked to the effect of strike-slip faulting at the SW tip of the North Anatolian Fault Zone in the Aegean on relatively stable crustal blocks in central Greece (*cf.* Goldsworthy *et al*. 2002). Palaeomagnetic measurements in the area (Markopoulo Basin) show $23.4^\circ \pm 11.9^\circ$ of clockwise rotation over the last 7 Ma (Bradley *et al*. 2013). Strain rates are among the lowest in entire Greece. Based on GPS observations, less than 50 nstrain a^{-1} have been assigned to northern Attica (Hollenstein *et al*. 2008; Chousianitis *et al*. 2013), which is in accordance with data from previous neotectonic studies. This strain rate corresponds to a horizontal extension of less than 1.75 mm a^{-1} across Northern Attica.

The graben of the Southern Evoikos Gulf marks the northern boundary of the study area. Active faults and extension are proven here (Papanikolaou *et al*. 1988b; Perissoratis & van Andel 1991). The Pliocene-Quaternary infill of the Southern Evoikos Gulf sums up to 250 m thickness (Papanikolaou *et al*. 1988b, 1989; Rondoyanni *et al*. 2007). It differs from the Northern Evoikos rift system in the Alpine geology, in fault slip rates and in GPS velocities. Furthermore, the Northern Evoikos Gulf encompasses warm springs and Quaternary volcanism which are lacking in the south.

A number of faults west of the Attica Detachment in the Sub-Pelagonian limestones have a clear topographic expression (*cf.* Papanikolaou *et al*. 1988a,b, 2008; Goldsworthy *et al*. 2002; Ganas *et al*. 2005). In the metamorphic units, at least two shorter faults are mapped. Most of these faults are in the order of 10–20 km in length and dip to the N(NE), only the southernmost ones close to Athens dip to the S(SW). Fault scarps testifying to Holocene activity are present in some cases. Papanikolaou & Lozios (1990) report that the faults east of the Attica Detachment are generally shorter and have lower slip rates. Judging from their mapped length and using empirical relationships, Ganas *et al*. (2005) estimate that the longest faults can produce earthquakes with magnitudes up to *M*6.6. However, the faults west of the detachment are also reported to have slip rates not exceeding 0.3 mm a^{-1} (Ganas *et al*. 2005; Papanikolaou & Papanikolaou 2007) based on tectono-morphological parameters, drainage network analyses and mapping (Fig. 1). Up to now, slip rates in the Attica region were not determined directly by palaeoseismological analyses.

Seismicity is low in the AMA (Papazachos 1990; Makropoulos *et al*. 2012) and among the lowest in entire Greece. Few historical events in the study area are known (Ambraseys & Jackson 1990; Papadopoulos *et al*. 2000b; Kouskouna & Makropoulos 2004), and archaeoseismological and palaeoseismological information is sparse (Stiros 1995; Stiros & Pirazzoli 1995) or focused mainly on the structural behaviour of buildings during seismic shaking (Mouzakis *et al*. 2002; Papantonopoulos *et al*. 2002; Psycharis *et al*. 2003; Psycharis 2007; Vayas *et al*. 2007). The three most significant earthquakes that we know of are the 1705, the 1938 and the 1999 events. From the 1705 event we do not know much except that it happened in the broader study area north of Athens and that it likely was not a major event (Ambraseys & Jackson 1997). The epicentre of the 1938 Oropos event is also somewhat uncertain and the earthquake could have happened at the Milesi Fault or at a longer fault to its north. Ground cracks occurred due to this earthquake at different faults, but it is not clear if any of them can be considered a coseismic rupture (see Goldsworthy *et al*. 2002 and references therein). As it is often the problem with old earthquakes (Pavlides & Caputo 2004), different catalogues of historical events report different data (magnitude/intensity, location and date). The September 1999 M_s 5.9 event occurred on the S-dipping Fili Fault (see Fig. 1: this event is marked by the grey fault plane solution west of the Athens Basin) according to Pavlides *et al*. (2002), but may have also been caused by another structure which does not reach the surface (Kontoes *et al*. 2000). However, the Fili Fault was not considered active before the event (Pavlides *et al*. 2002) and if there is another fault close-by it was unknown.

2.3 Seismic hazard

In the seismic hazard zonation of Greece, zone I represents the lowest and zone II refers to an intermediate seismic hazard. The western section of the broader study area belongs to seismic hazard zone II; the east is categorized as zone I (Fig. 1, EAK 2003). This is remarkable in that the boundary between the two hazard zones crosses several active faults. The result is that cities and villages in zone I have a less strict building code than those in zone II, despite the fact that they are at similar distances from the same fault. For example, the village of Eretria belongs to zone II and Amarinthos in southern Evia belongs to zone I (EAK 2003), but both locations are at the same distance from the faults in the Southern Evoikos Gulf (Papanikolaou *et al*. 1989) and those in Northern Attica (Goldsworthy *et al*. 2002). The study area comprises villages and small cities only (population of Oropos Municipality: 33 800;

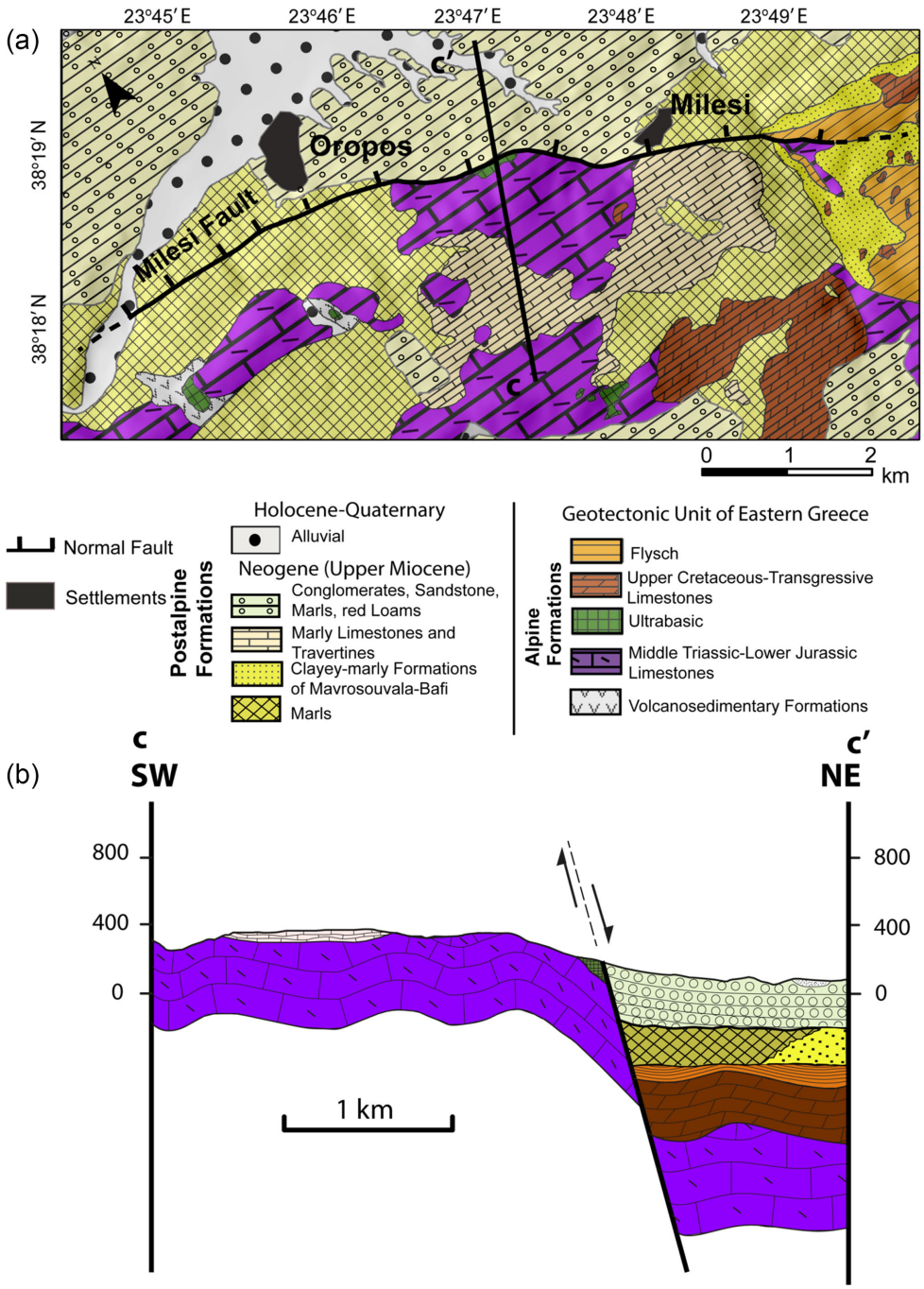

Figure 3. (a) Geology of the Milesi Fault and the surroundings (after Katsikatsos 2000). The garbage dump site is located at the ultrabasic rock outcrop. C–C′ marks the cross section in B. (b) Cross section based on the Geological Map (Katsikatsos 2000). The total throw of the Milesi Fault is 1050 ± 500 m.

Eretria: 13 000; Amarinthos: 10 000; Kalamos: 3700) and no major industrial complexes are located here. However, in the summer, the population of Athens drops by 16 per cent while that of the rest of Attica increases by 58 per cent (Avramidou *et al*. 2009). Therefore, during the summer months the population of the study area increases significantly and there is an obvious need for a reliable seismic hazard assessment.

2.4 Study site

The Milesi Fault is located about 30 km north of Athens. It is an ESE–WNW striking, N-dipping normal fault with a length of around 10 km. The densely populated Oropos plain is located to its north. The footwall of the fault is mainly made up of Triassic-Jurassic limestones (Fig. 3a). A pocket of ophiolites stemming from thrusting and nappe stacking during the Alpine collision is present west of the Milesi village. There, a garbage dump has been built recently and the colluvium and parts of the ophiolite footwall have been removed by excavators. The hangingwall of the fault consists of colluvium, marls, conglomerates and loams. Few landslides have been identified in the Neogene soft sediments in the gentle hills north of the fault zone. No landslide is known from the vicinity of the garbage dump site. Deeply incised channels are visible in the footwall. The elevation difference between the footwall

and the hangingwall is up to 300 m. The accumulated net offset of the fault is not precisely known. From cross sections based on the official 1:50 000 scale geological map (Katsikatsos 2000) it is clear that its finite (total) throw is 1050 ± 500 m. The large error bar stems predominantly from the uncertainty regarding the thickness of the postalpine sediments which vary significantly over short distances (Fig. 3b). Papanikolaou *et al*. (1988a) concluded from geomorphological studies that the Milesi Fault is likely active. This would mean that it could probably produce an earthquake similar to the 1938 or 1999 events. Therefore, the Milesi Fault is an ideal test site to investigate its slip rate by palaeoseismological studies.

3 METHODS

In order to investigate the Milesi Fault's activity, we combined remote sensing techniques with geophysical investigations, classical field mapping and palaeoseismological trenching and dating.

3.1 Geomorphological analyses

Repeated normal faulting events generally produce elevated mountains on the footwall of the block and lead to the formation of basins on the hangingwall. Depending on the interaction between tectonic activity and erosion/sedimentation, relatively linear mountain fronts could form. Their height is determined by the cumulative throw. An ideal normal fault will lead to a maximum offset in the central sector of the fault zone and to zero offset at its tips. In the field, this arc-shaped feature is rarely perfectly preserved (*cf.* McCalpin 2009). Often it is hard to determine where the centre of the fault zone is and where the maximum offset is located. Since palaeoseismological investigations aim on determining coseismic offsets and slip rates, it is important to ensure that trenching either takes place where the offset is maximum or that corrections are applied when offsets and slip rates are determined closer to the tips of the fault.

A classified description of the visible throw based on the topographic variations, that is a part of the finite throw, can be used to estimate best possible sites for field measurements and trenching. Using a new GIS-based approach, we classified those zones into four categories along the fault, assuming that high visible displacements correlate with palaeoseismological surficial expressions. ArcGIS was used for these calculations. A digital elevation model (DEM) was derived from the 20 m contour data of the 1:50 000 topographic map of the Hellenic Military Survey. The DEM is based on 20 × 20 m cells (Fig. 4a).

190 attached and parallel polygons, each of 50 m width, operated as samples for elevation measurements. The watershed was defined to be the mountain ridge and thus, the peak elevation per polygon along the footwall (Fig. 4b). We used the fault trace from the geological map of Katsikatsos (2000) and determined the altitude along fault strike from the DEM. Minimum and maximum elevations per sample along the fault were calculated as well as the derived spread (Fig. 4c). Then the spread was categorized in 25 per cent-quantiles from the maximum difference (Fig. 4b).

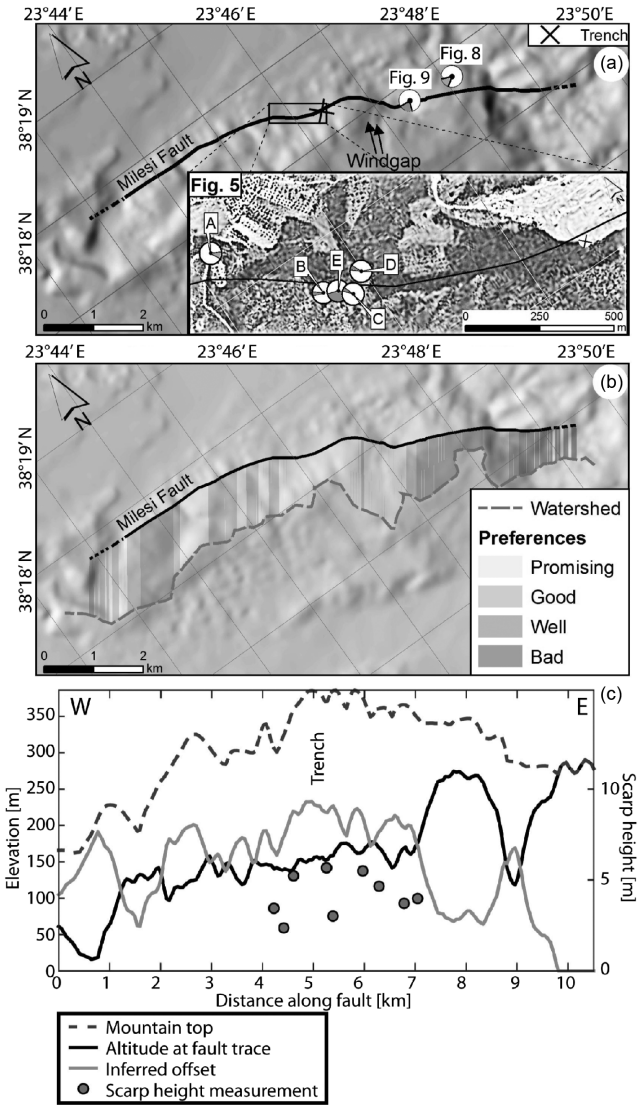

Figure 4. (a) Detailed local map of the Milesi Fault with the position of the trench, the photos of Figs 5 and 8 (grey circle sectors indicate direction), and the two mapped windgaps. Elevation data are based on 20 m contour data. Inlet shows GoogleEarth imagery of the trench site at the garbage dump. (b) Results of the DEM-based geomorphological analysis described in Section 4.1 with vertical grey stripes indicating suitability for palaeoseismological analyses: Light grey = more suitable, dark grey = less suitable. (c) Data used for the geomorphological analysis. Visible offset is the elevation of the mountain top minus the elevation of the surface outcrop of the fault. This value indicates the lower boundary of possible throw along strike, as it does not account for erosion. The rate of visible throw versus total throw is estimated to be in the order of $^1/_2$ to $^1/_4$. Thus, the inferred offset is only a portion of the total throw. The figure illustrates the distribution of offset along strike. Dots are scarp heights measured in the field. Note that one dot may represent more than one measured value when distance between measurement locations was small and values did not change significantly.

3.2 Field mapping

We mapped the height and orientation of the visible postglacial fault scarps along the fault strike (Fig. 5). Sites with possible mass movements at the fault scarp were identified for avoiding a misleading interpretation of observed offsets. Topographic profiles crossing the fault scarp were collected by means of a yardstick and an inclinometer in order to identify the total postglacial throw. Near the village of Milesi, we investigated two deeply incised channels that cut into the footwall and mapped the source area of the corresponding streams. This was done for evaluating if tectonic uplift possibly caused the abandonment of the streams, resulting in windgaps. Field mapping

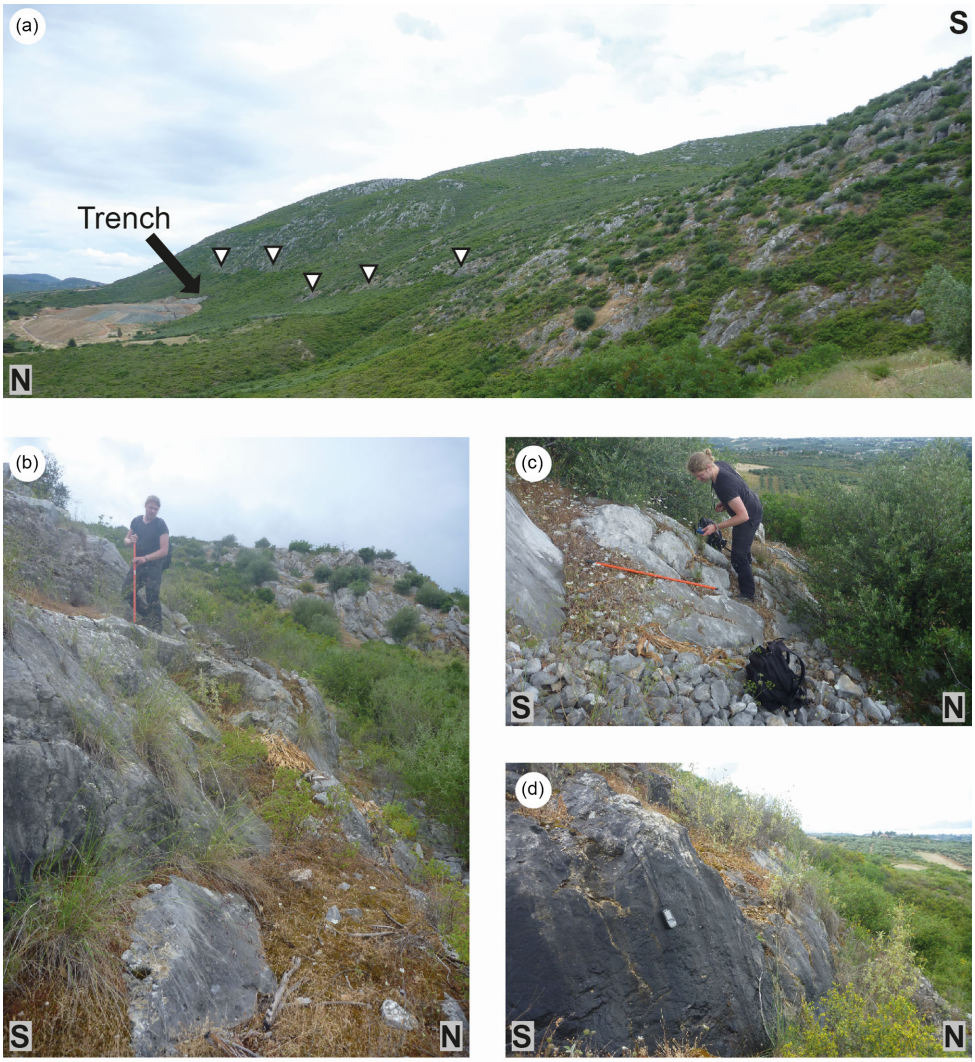

Figure 5. Photo plate illustrating the different types of scarps mapped in the field. See Fig. 4 for location. (a) Panoramic view across the central part of the Milesi Fault from the west. White triangles indicate scarps mapped at different elevations. Note that the trench lies in the continuation of the lower scarp, indicated with the three triangles to the right, as described in Section 4.2.1. The two triangles in the left indicate the large plane as described in Section 4.2.2. (b) Segmented scarp dipping ∼60° to the north, with a smooth surface and kinematic indicators. The dip angle varies at this site, and total offset was determined by averaging over the entire outcrop. Most of the steps visible are break outs along Riedel shears. (c) Polished scarp dipping to the north with 50°, kinematic indicators point to pure normal movement, note the step in the fault plane and the deep cracks in the lower plane. (d) Degraded scarp dipping 80° to the north, note that the surface is not as polished, still corrugations as slip indicators are visible. GPS for scale is 0.13 m. The scarp locally bends from E–W to SE–NW strike, following the mountain front, but dips to the north in general.

results were used to determine locations for later geophysical surveys and trenching.

3.3 Palaeoseismological trenching

A garbage dump site was recently established west of the Milesi village. During field mapping we found that the hangingwall and the footwall were excavated, exposing the fault and hangingwall deformation structures. We enlarged the existing outcrop in order to make it a suitable palaeoseismological trench. The trench walls were levelled manually and we deepened the most interesting parts of the trench. After that the trench walls were cleaned and a square metre grid was attached. The trench was sketched in 1:10 scale. We photographed the outcrop for creating a digital mosaic with image processing software. A retrodeformation was performed in order to provide a possible explanation for the observed deformation and to identify surface-rupturing seismic events. Palaeosols and colluvial wedges were sampled for radiocarbon dating. Eight bulk samples were taken, four of which were sent to the Beta Analytic laboratory for dating.

3.4 Geophysical profiling

A ground penetrating radar survey (georadar, GPR) was conducted for identifying hangingwall deformation along the fault strike. Aim of these measurements was to verify that the features observed in the trench are not limited to one location only, but can be traced along the entire central sector of the Milesi Fault. We measured several profiles on top of the trench and in its immediate vicinity. Unfortunately, the GPR survey with a 400 MHz shielded antenna system did not produce non-ambiguous data and we therefore do not present the results here. The dense vegetation (Maquis shrubland)

and the uneven surface are regarded as possible reasons for the low data quality. The presence of a large number of boulders in the subsurface further complicates the identification of lithological units.

4 RESULTS

4.1 Geomorphological analysis

The analysis of the DEM resulted in a categorization of the fault zone in terms of favourable sites for detailed field investigations. Four classes were calculated, ranging from 'promising' to 'bad' for field work, based on the inferred throw of the fault (Fig. 4b). The inferred offset noted in Fig. 4(c) is not the total offset, but simply the topographic offset which is only a portion of the total throw. The difference in the topography along fault varies between 0 m in the east to 240 m at the centre. In the west, the visible topography reaches 100 m. Assuming a ratio for visible throw versus total throw of $^1/_2$ to $^1/_4$ implies that the max throw should be in the order of 720–1200 m (using the 240 m of maximum topographic offset), which fits very well with our cross section that shows the total throw. Based on the analysis of elevation data (Fig. 4c) the most promising sites for field measurements are located at the centre of the fault (Fig. 4b). Here the highest slip rates can be expected. Hence, the Milesi Fault can be categorized as a symmetrical normal fault. This is a hint for normal fault movement with no substantial oblique-slip. Within good-promising categorized zones we found surficial expressions (postglacial fault scarps with kinematic indicators) and also the artificial trench at the garbage dump close to Milesi village.

4.2 Field mapping

Hard rock scarps were mapped in the limestones along the entire fault (Fig. 5). All mapped scarps were mainly oriented E(SE)–W(NW). Kinematic indicators were found on some of the scarps, although in such bad state of preservation that no precise measurements were possible. Fault plane corrugations, however, point to almost pure normal movement with a slip vector pointing approx. to the north. No systematic oblique-slip component was observed. The mapped features can be classified in two different sets based on their dip and overall dimension: Steep dipping scarps with small offsets and large, shallower dipping fault planes (Fig. 6a).

4.2.1 Steeply dipping scarps

To the west of the garbage dump, up to three different scarps within few tens of metres horizontal distance were recognized, showing a staircase-like pattern with cumulative heights ranging between 3 and 5 m (Figs 5a–d, see Fig. 4 for location, and Fig. 6a for an overview). The observed total vertical throw slightly increases towards the centre of the fault. Dip angles vary between 40° and 80° to the north, most of them are around 60° (Fig. 6b). One of these scarps marks the continuation of the fault observed in the trench (Fig. 5a). The scarps are partly polished and a thin breccia sheet was observed in various places.

No mass movements were observed in any of the sites where the scarps were mapped, and no hint for mass movements could be found at the trench site. Most scarps show kinematic indicators typical for normal movement such as Riedel shears and tension gashes (Doblas 1998). Remains of slickensides have been found,

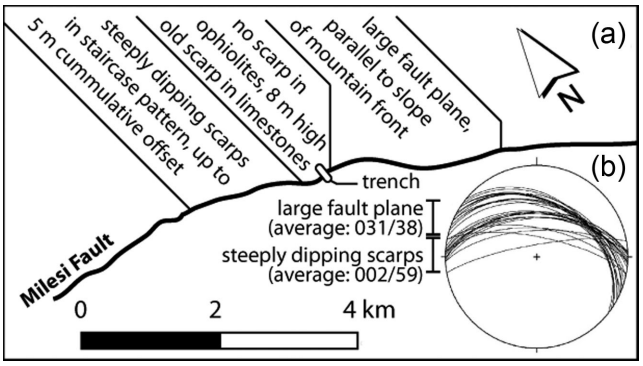

Figure 6. Generalized overview of the mapped features. (a) Along the strike of the fault, three zones can be distinguished. Steep dipping scarps are present in the limestones west of the trench site. No scarps were observed in the ophiolites at the trench site, but a large fault plane was found in the limestones above the trench (see Figs 5a and 7). Large fault planes are present east of the trench site (Figs 8 and 9b). (b) The great circle diagram illustrates the two different classes of scarps that can be distinguished: large fault planes dipping to the N(N)E and steeper dipping scarps towards the north as described in Sections 4.2.2 and 4.2.1, respectively.

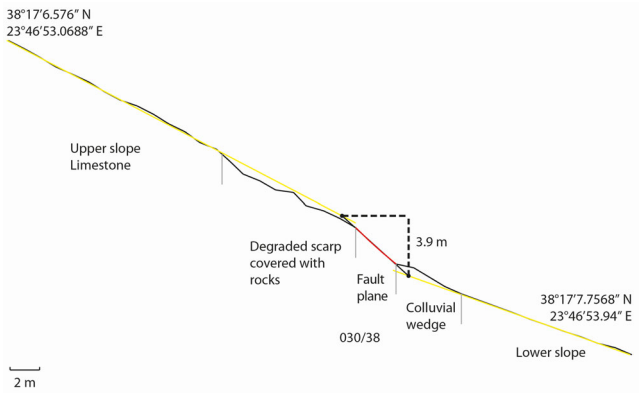

Figure 7. Topographic scarp profile of the weathered large fault plane above the trench site. This fault plane dips with 38° to the NNE (30°/38°) and shows a vertical throw of 3.9 m as derived from the profiling by means of a yardstick and an inclinometer for methodology see Papanikolaou *et al.* (2005). Coordinates indicate the upper and lower ends of the profile.

but no slip vector could be measured because they were either too weathered or not in-situ.

4.2.2. Large fault planes

Above the trench site a fault plane 8 m wide and 60 m long is located. This plane has a dip angle of 38° towards the NNE (30°/38°). Strong degradation and intense karstification indicate it is older than the others. Fig. 7 illustrates a topographic profile measured across this structure for determining the total vertical throw, which is 3.9 m. We used this method to measure the scarp heights along the entire fault trace.

East of the trench site, not a set of scarps but one major fault plane was observed. It shows a dip of 30°–40° to the north (*cf.* Figs 6–8 and 9b). The surface of this plane is very smooth. The slope angle is the same as the dipping angle of the limestone hardrock surface close to the trench and east of this site. The mountain slope is broadly defined by this fault surface. Kinematic indicators include Riedel shears and tension gashes, indicating normal movement. As the plane was slope-parallel, it was impossible to retrieve scarp

Figure 8. The Milesi Fault plane cropping out east of the garbage dump and trench site, close to Milesi village. See Fig. 4 for location, view is to the west. The fault plane is several metres in height and makes up the entire lower part of the mountain front. The average dip direction is north and the dip angle here is around 55°. The two windgaps are located behind the last arrow to the right. Local mass wasting processes are likely to have exposed a large part of the fault plane here and no palaeoseismological data were collected.

heights in terms of vertical offsets. No scarps were observed in the ophiolites.

Fig. 6(b) shows great circles of the general strike and dip directions of the mapped scarps. The data group in two distinct sets, representing the large angle fault planes and the steeply dipping scarps, respectively.

Deeply incised channels (Fig. 9) a few hundred metres west of the village Milesi were observed. They do not to reach the base of the slope, but seem cut by the fault scarp around 5 m above the hangingwall level. This indicates that either fault activity (footwall uplift) is faster than incision or that the stream has been abandoned by tectonic movements, upstream mass movements, or anthropogenic influence. Papanikolaou *et al*. (1988a) already reported on the intense incision of this stream. We mapped the streams' source area and found that both streams were not deviated by mass movements or influenced by human activity. The catchments of both streams are located on the top of the footwall mountain range and lack a large source area. The deep incision of the streams must have occurred earlier, when the hydrographic basins were larger before tectonic uplift. The fact that the streams do not reach the hangingwall level therefore suggests relatively recent (postglacial) fault slip. Accordingly, both incised channels could be interpreted as wind gaps. Analysis of digital elevation data and aerial imagery supports the field observations (Figs 9a and b).

The profile of the fault escarpment upslope the scarp has a convex shape (Fig. 7). This shape can be explained by the model of scarp degradation, thus testifying to ongoing tectonic offset at the fault and subsequent erosion/degradation of the footwall (see Hamblin (1976) for the general concept and Stewart & Hancock (1988) for degradation models in the Aegean region and references therein).

4.3 Palaeoseismological trench

Palaeoseismological trenching generally aims at identifying and dating units that are offset by fault movement. Age control is usually done by radiocarbon dating if suitable organic material like charcoals, plant remains, etc. is present. Palaeosols do often contain enough bulk organic material to be dated, even if distinct pieces of organic matter cannot be retrieved. Furthermore, palaeosols are excellent markers for reconstructing the horizons that were the surface in the past, later downthrown by fault movement and buried by younger material from the footwall of the fault. In this section, we describe the palaeosols that have been found in the trench and provide detailed information on the units present in the hangingwall.

The outcrop at the garbage dump site reveals the contact between the ophiolites in the footwall and the colluvium, separated by a shear

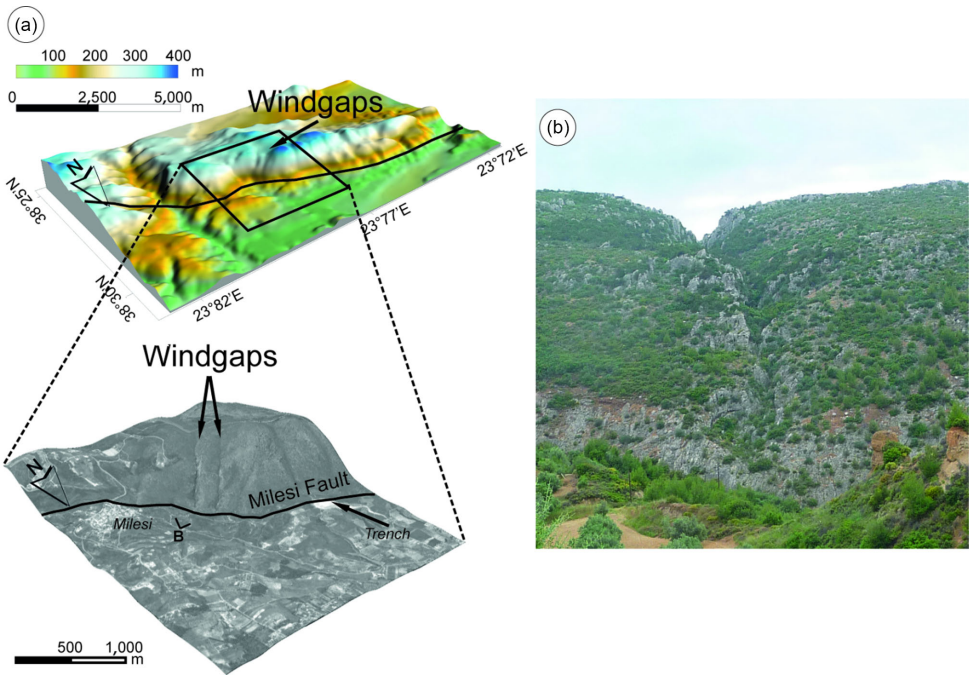

Figure 9. (a) Digital elevation model of the study area derived from 20 m contour lines (upper image) and the GoogleEarth satellite image prove the existence of at least two windgaps at the Milesi Fault. (b) The deeply incised streams do not reach down to the hangingwall, but stop at the crest of the fault scarp. There, the scarp is ∼5 m high.

zone dipping to the N (Fig. 10). The greenish-yellowish ophiolites in the footwall show internal shear structures. The contact between the sheared ophiolites and the non-sheared ophiolite gravels dips roughly ~75° the north. The hangingwall is made up of alternating layers of colluvium, colluvial gravel wedges and palaeosols (Figs 10 and 11). Almost all colluvial layers do not show distinct boundaries, but a rather smooth change in colour and composition (Fig. 10). The boundaries of palaeosols and gravel layers are more well-defined. Gravel wedges and the palaeosols can be identified clearly. The lowermost colluvial unit (units U1a and U1b in Fig. 11) is 0.6–0.8 m thick and consists of brownish to whitish-brownish, silty fine-medium sand with fine gravels. It is overlain by an eye-catching red palaeosol layer 0.15 m thick, P1. Palaeosol P1 has an apparent dip angle of ~45° to the north in the northern parts of the outcrop. Within two metres distance from the fault zone, the inclination is shallower (~26°).

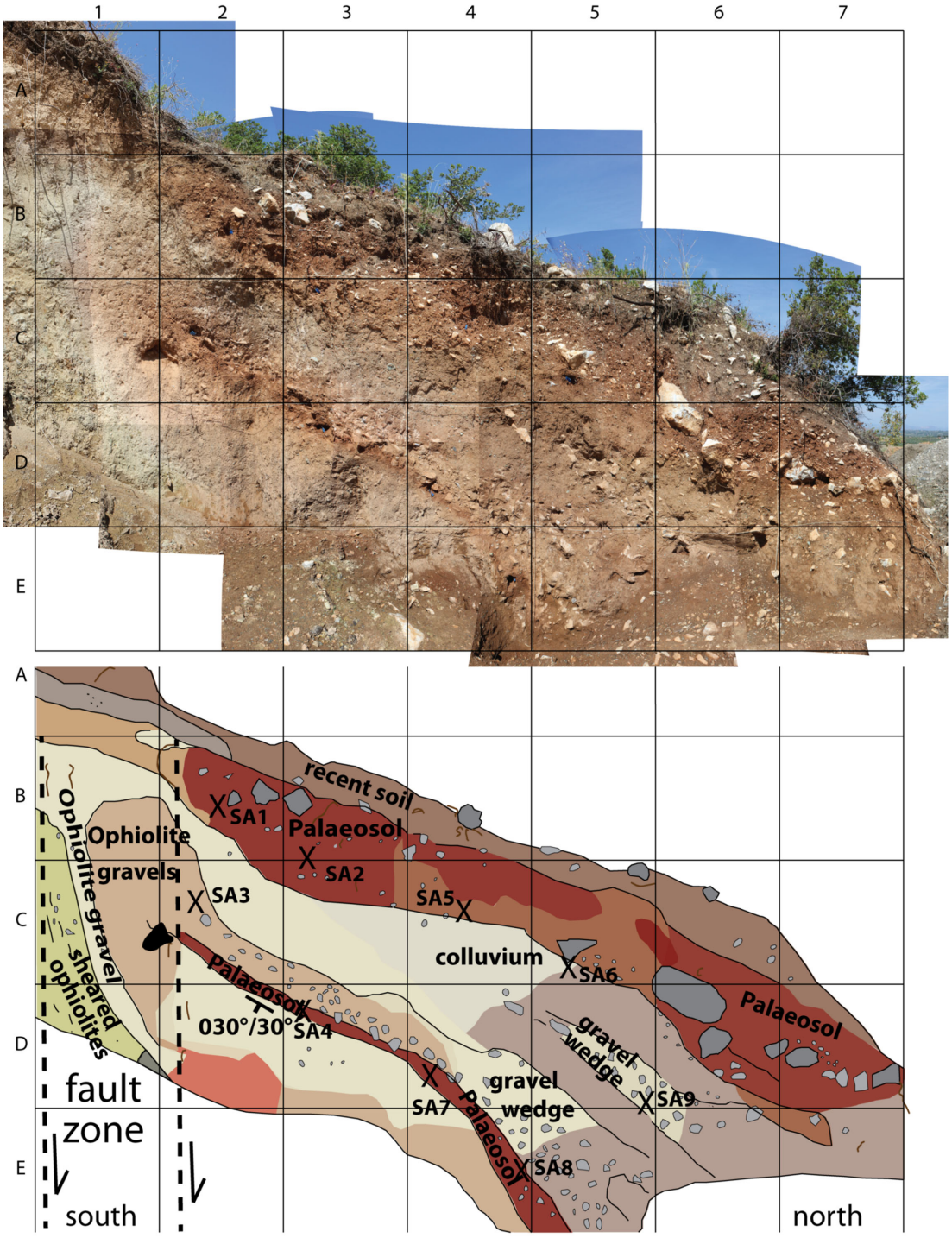

Figure 10. Photo mosaic of the trench at the garbage dump (upper image) and sketch of the main units (lower image). Grid width is 1 m. Note the buried palaeosol close to the surface and a second one at 1–2 m depth. SA: Sample location. 030°/30°: dip direction and dip angle of the second palaeosol.

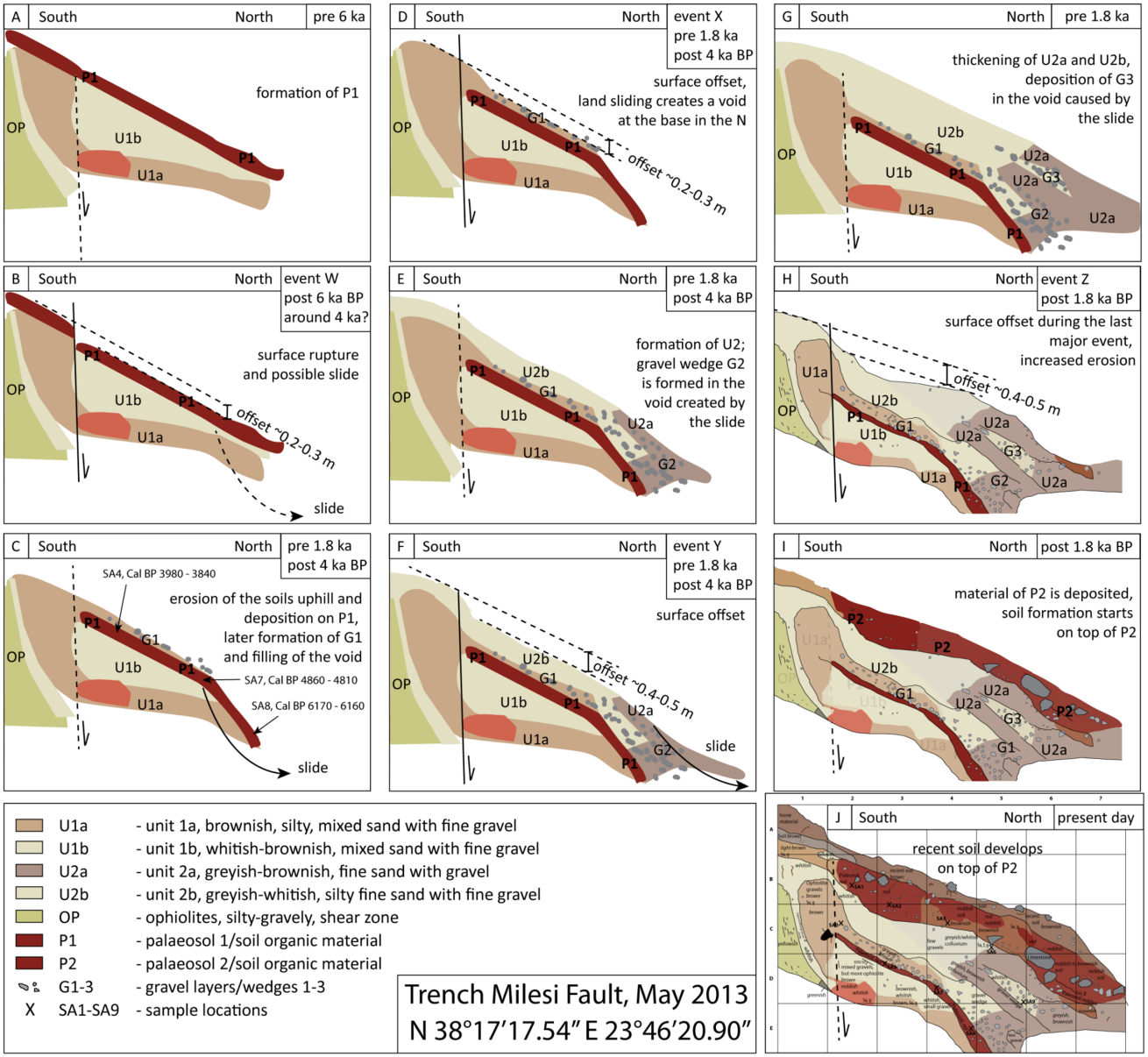

Figure 11. A possible retrodeformation for the palaeoseismological trench at the Milesi garbage dump with four, maybe even five earthquake events that led to the present day geometry. Ages drawn into the sketch represent the dating results.

On top of the palaeosol we found colluvial units U2a and U2b as well as three gravel wedges (G1–G3). These two colluvial units are not overlying each other, but instead interfinger and are characterized by different colours and grain size distributions. U2a is a greyish-brownish fine sand with gravel. This unit is only present in the northern part of the outcrop and has a thickness of up to 2 m. U2b consists of greyish-whitish, silty fine sand with fine gravel and it is almost 1 m thick. Gravel wedge G1 overlays the aforementioned steep dipping palaeosol P1 and ends at the knick point. The wedge is 0.5 m thick in its northernmost part and characterized by sub-angular to angular mixed limestone gravels. Gravel wedge G2 overlays palaeosol P2 and has an average thickness of 0.15 m. It ends close to the shear zone and also consists of mixed limestone gravels of sub-angular to angular shape. G2 appears to be embedded in a colluvial layer with the same properties as U1a. Gravel wedge G3 is embedded in U2a. It is located about 1 m north of the eye-catching knick point of P1. It thickens towards the north up to 0.3 m. It consists of mixed limestone gravels of sub-angular to angular shape in a matrix of greyish-whitish silty fine sand.

Another palaeosol (P2) is present on top of those colluvial units and it is covered by the actual soil. P2 has a thickness of almost 1 m in the northernmost parts of the trench and about 0.5 m in the central part. Large blocks and few gravels are incorporated in a reddish fine grained matrix.

Radiocarbon dating of P1 was performed for samples SA4, SA7 and SA8 (Fig. 12). From the upper palaeosol P2 sample SA2 was dated (Fig. 11; Table 1). All samples were dated by Beta Analytics and calibrated (2σ calibration and OxCal V4.2.3 using IntCal13; Bronk Ramsey 2009; Reimer *et al.* 2013). The results revealed that the upper (southern) part of the lower palaeosol (P1) yields an age of *ca.* 4000 a. Its middle part is roughly 1000 a older while the northernmost sample has an age of ~6000 a. This fact implies that P1 is made up of different components, possibly reworked and affected by younger soil forming processes

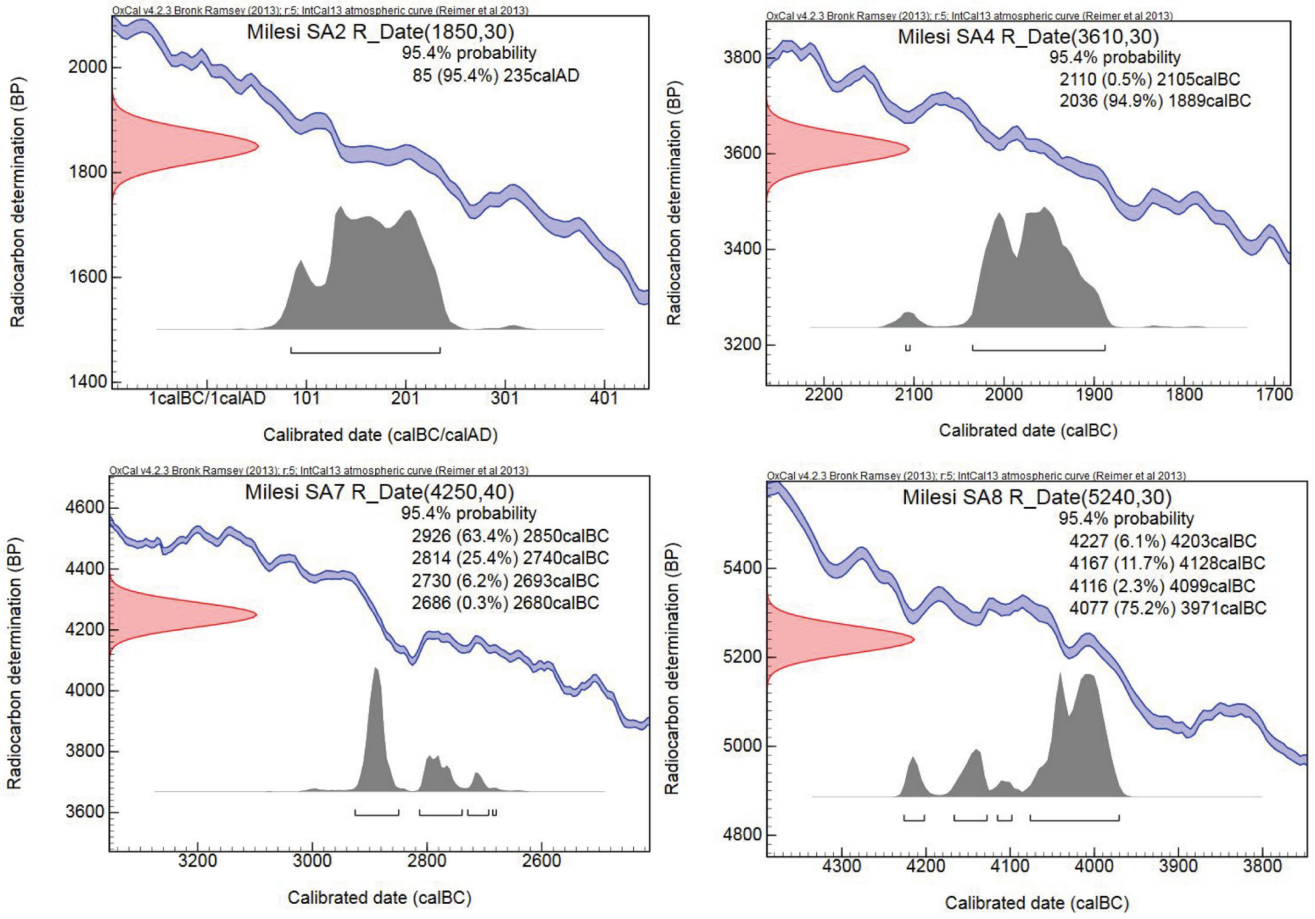

Figure 12. Dating results of the four samples SA2, SA4, SA7 and SA8, after calibration with OxCal using IntCal13. Images are from the OxCal website.

Table 1. Dating results for the four samples from the trench.

Sample	Material pretreatment	Measured age / conventional age	13C/12C	2σ Calibration	Calibrated age (OxCal, IntCal 13)
Milesi SA2	Organic sediment: acid washes	1850 ± 30BP	−25.1 o/oo	Cal AD 80 to 240 (Cal BP 1870 to 1710)	AD 85–235
Milesi SA4	Organic sediment: acid washes	3610 ± 30 BP	−24.7 o/oo	Cal BC 2030 to 1890 (Cal BP 3980 to 3840)	2110–1889 BC
Milesi SA7	Organic sediment: acid washes	4250 ± 40 BP	−25.0 o/oo	Cal BC 2910 to 2860 (Cal BP 4860 to 4810) AND Cal BC 2800 to 2760 (Cal BP 4760 to 4710) Cal BC 2720 to 2710 (Cal BP 4660 to 4660)	2926–2680 BC
Milesi SA8	Organic sediment: acid washes	5240 ± 30 BP	−24.8 o/oo	Cal BC 4220 to 4210 (Cal BP 6170 to 6160) AND Cal BC 4160 to 4130 (Cal BP 6100 to 6080) Cal BC 4060 to 3970 (Cal BP 6020 to 5920)	4227–3971 BC

after its initial formation. The upper palaeosol P2 has an age of ∼1800 a.

5 INTERPRETATION

5.1 Geomorphological analysis

The geomorphological analysis showed hints for relatively recent fault movement. The deeply incised canyons which are cut at the base suggest that vertical fault movement occurred faster than erosion. No hints for mass movements could be found at this place, so coseismic offset is a likely explanation for this observation. Furthermore, the presence of two windgaps is a sign for on-going tectonic uplift of the footwall of the Milesi Fault, thus neotectonic activity, as already pointed out by Papanikolaou *et al*. (1988a).

5.2 Field mapping

If a postglacial age is assumed for the observed fault scarps (e.g. Benedetti *et al*. 2002; Papanikolaou *et al*. 2005), the observed throw occurred during the last 15 ± 3 ka. For the set of steeply dipping scarps with a total height of *ca.* 5 m we calculate an average throw

rate of 0.33 +0.08/−0.06 mm a^{-1}. The 3 m high set of staircase-like scarps would correspond to 0.2 ± 0.05 mm a^{-1}.

The topographic profile across the weathered scarp at the garbage dump site would similarly imply 0.26 ± 0.06 mm a^{-1} average throw rate during the last 15 ka. However, the scarp is intensely degraded and shows much more karstification than any other of the mapped structures, despite the lithology is the same. This means that it has been subject to erosion for a longer time and it was not polished by recent fault movement. There are two possible explanations. (1) The entire offset measured here occurred in a shorter time period after the last glacial maximum (LGM), and stopped relatively shortly afterwards. Then, the slip rate would have been much higher in this short time period; (2) the weathered scarp might be an even older, pre-LGM feature. In both cases the offset cannot be used to infer a Holocene slip rate and we will not consider this value in the following reasoning.

The large fault plane east of the garbage dump (Fig. 9) shows that the streams did not erode the lowermost 5 m. If this amount represents the slip since the LGM, the throw rate would be in the order of 0.33 +0.08/−0.06 mm a^{-1}. All these rates must be considered minimum values as erosion and sedimentation might have lowered the offset visible in the field.

We consider the large, slope-parallel fault plane with a dip of ∼38° as relatively older compared with the steep scarps and probably backward tilted during repeated faulting. We interpret the smaller and steeper scarps to have been created by cracking and extension during faulting, thus representing deformation in the limestones of the hangingwall above the fault plane. This implies that coseismic ruptures can occur at various sites along the fault, but are not necessarily confined to one single fault scarp.

We encountered no scarps in the ophiolites, but only in the neighboring limestones. This is ascribed to a much lower resistance to erosion within the ophiolites. Fig. 10 illustrates that these rocks are intensely sheared and heavily degraded in the fault zone.

5.3 Trenching

Fig. 11 illustrates a possible retrodeformation of the trench. There is no hint for any anthropogenic activity within the exposed geological units, thus we take into account natural processes only. We propose that at least four surface rupturing earthquakes lead to the present day geometry during the last 6 ka (Figs 11a–j), successively downthrowing the palaeosols and being followed by periods of sedimentation. We suppose that the colluvial wedges are associated to the downthrow. Directly after the seismic event space was available for the wedges to form and likely loose material was available upslope due to the shaking. A possible explanation for the kink in P1 and the layers above are shallow slides (Figs 11c and f). Although we carefully examined the trench for any features related to sliding and did not encounter any hints, we cannot rule out such processes.

The lowermost palaeosol P1 has components which are between 6000 and 4000 years old and it is currently located at 1.8 m depth. The difference in the age suggests that probably reworked material from upper parts of the slope is incorporated in this layer, and that after initial formation further soil forming processes took place. However, no date is younger than 4 ka, so we assume that P1 was downthrown and buried around that time. This would correspond to an average throw rate of ∼0.45 mm a^{-1} over the last 4 ka. If 0.2 m of recent soil formation are assumed, the throw rate would be in the order of 0.4 mm a^{-1}. These rates are slightly higher than the ones calculated from scarp mapping. Our interpretation of at least four events that lead to the downthrow of P1 within 4 ka indicates an average recurrence interval of 1000 yr, or 1500 yr if the age of 6 ka is assumed.

Palaeosol 2 likely consists of in-situ soil and colluvial material from the upper part of the slope, judging from the amount of gravels found in this layer and its thickness. This layer is located at an average depth of 0.5 m below surface and yields an age of ∼1800 yr. Assuming that this is a minimum age, a throw rate of 0.28 mm a^{-1} over the last 2 ka can be assumed.

It is not possible to precisely reconstruct the amount of erosion and sedimentation that might have taken place at each stage of the geological history. The obtained slip rates are, however, in the same order as those calculated from topographic profiling and those obtained at neighbouring faults with similar size (Ganas *et al*. 2005; Papanikolaou & Papanikolaou 2007). It must be noted that the numbers derived from scarp profiling are minimum values. The average throw per event appears to be 0.2–0.5 m. As the trench is located close to the centre of the fault this represents a maximum value. The slip per event cannot be determined more precisely, again due to the fact that the amount of sedimentation and erosion in between the seismic events can only be estimated. However, such displacements can be expected based on empirical relationships and the fault rupture length (Wells & Coppersmith 1994; Ambraseys & Jackson 1998; Pavlides & Caputo 2004).

The average fault dip at depth cannot be unambiguously determined from the dip angles of scarps at the surface. No constraint on the average dip of the Milesi Fault from seismological observations is available due to the absence of sufficiently strong earthquakes during the last ∼100 years. Ambraseys & Jackson (1990) assume a 45° N-dipping fault plane for the Oropos earthquake of 1938. It is known that the dip angles observed at the surface are often steeper than those at depth, which also seems to be the case in the broader study area (Stewart & Hancock 1988). Most normal faults in extensional regimes appear to have dip angles of 40–60° (Jackson & White 1989). The large fault plane that we mapped has an average dip of 38° only, the smaller fault scarps dip with 40–80° (60° on average). We use an average dip of 45° for our further calculations.

6 FAULT SPECIFIC SEISMIC HAZARD ASSESSMENT OF THE MILESI FAULT: EARTHQUAKE SCENARIO

Seismic hazard assessment tends to follow fault specific approaches where seismic sources are geologically constrained active faults (WGCEP 2002; Boncio *et al*. 2004; Roberts *et al*. 2004; Pace *et al*. 2010; Papanikolaou *et al*. 2013; SHARE Project 2014). The aim is to address problems relating to the incompleteness of the historical records since geological data sample much greater periods of time and obtain higher spatial resolution and realistic source locality distances, because seismic sources are accurately located. Fault specific approaches are becoming very important for seismic hazard assessment, by providing quantitative assessments through measurement of geologically recorded slip on active faults (Michetti *et al*. 2005). Based on slip-rate data and the fault geometry, seismic hazard maps can be constructed purely from geological data (Papanikolaou 2003; Roberts *et al*. 2004).

In order to evaluate the consequences of seismic events typical for the Milesi Fault, we developed an earthquake scenario. Our aim is to visualize recurrence intervals for maximum intensities to be expected from seismic events at this fault.

6.1 Input parameters

Magnitude scaling relationships were used to estimate the magnitudes of the palaeo-events. The observed maximum displacement of 0.2–0.5 m and a fault length of 9.7 km fits well to the relationship of Scholz *et al*. (1986). Assuming a seismogenic thickness of 10–15 km, a dip angle of 45° and a rigidity of $\mu = 3 \times 10^{10}$ N m^{-2} results in a seismic moment of 8.2–31 $\times$ 10^{17} Nm, which corresponds to magnitudes of M_w 5.9–M_w 6.3. If we assume possible surface ruptures of the entire fault length (9.7 km as mapped in the field), the maximum magnitude according to Wells & Coppersmith (1994) and Pavlides & Caputo (2004) would be *M*6.2. The relationships of Ambraseys & Jackson (1998) result in M_s 6.2–6.5 based on the offset and ~M_s 6.3 based on the fault length. We decided to use a moment magnitude of *M*6.2 as input parameter for the earthquake scenario. Based on the trenching result, we also assume a recurrence interval of 1000–1500 a for these events.

The method of seismic hazard mapping from geological fault throw-rate data consists of the combination of the following major factors for each active fault (Papanikolaou 2003; Roberts *et al*. 2004):

(1) Empirical data which combine fault rupture lengths, earthquake magnitudes and coseismic slip relationships (Wells & Coppersmith 1994; Pavlides & Caputo 2004);
(2) The radiuses of VII, VIII and IX isoseismals on the Modified Mercalli (MM) intensity scale, within which horizontal ground accelerations exceed 5 m s^{-2} in the Greek territory (Theodulidis & Papazachos 1992) causing damage even to well-constructed buildings (Reiter 1990);
(3) Attenuation—amplification functions for seismic shaking on bedrock compared to basin filling sediments (Degg 1992).

We assumed a 45° dipping fault plane, based on the field mapping and taking also into consideration that seismogenic faults on the continents appear to be restricted to a dip range between 30° and 60° (Jackson & White 1989; Chen & Molnar 1983). The hypothetical epicentres were plotted 10 km away from the fault trace in the hangingwall, assuming hypocentral depth of 10 km. We plotted 14 km radius isoseismals for intensity VIII, 29 km radius for intensity VII isoseismals and 51 km for intensity VI (MM) isoseismals based on the Theodulidis (1991) attenuation relationships between earthquake magnitude and intensities distribution. The modelled intensities were then amplified/attenuated according to the local geology. The Quaternary deposits increase the intensity by one degree; the flysch/Neogene deposits caused no alterations, while the bedrock (mostly Mesozoic or Tertiary limestone) decreases the intensity by one degree.

6.2 Site dependent intensity distribution

The final seismic hazard map (Fig. 13) shows the spatial distribution of the maximum intensities expected by the re-activation of the Milesi Fault ranging from intensity VII to IX after considering the amplification due to the surface geology. Therefore, this map offers a locality specific shaking recurrence record. Fig. 13 illustrates how many times each locality received enough energy to shake at its maximum expected intensity (VII, VIII or IX) over the past 15 $\pm$ 3 ka, assuming a circular pattern of energy release. Highest hazard is observed, as expected, towards the hangingwall centre of the Milesi Fault and diminishes towards the tips, following the slip-rate variability along strike the fault. The highest shaking frequency over the past 15 $\pm$ 3 ka is 14, implying that this area will experience intensity IX from the Milesi Fault every 1070 $\pm$ 220 yr.

It is interesting to note that significant damage is expected also on the northern side of the Southern Evoikos Gulf on the island of Evia, where the coastal towns of Eretria and Amarinthos are situated. Settlements founded on Holocene alluvial and coastal sediments are regarded as highly vulnerable and under certain circumstances could experience even intensity X and extensive liquefaction phenomena. We emphasize herein that this hazard is posed solely from the Milesi Fault and does not represent the cumulative hazard from neighbouring faults. Also, we do not claim that our simplified seismic hazard map should replace the official ones published by EAK (2003), but it illustrates the problems and weaknesses associated with the presently used approach of seismic hazard zonation.

7 DISCUSSION

7.1 Uncertainties in the historical earthquake catalogue

The comparison of different sources for historical earthquake data shows that significant discrepancies exist. Catalogues may be incomplete or ascribe erroneous data to earthquakes. The epicentral location of single events vary significantly within different catalogues (e.g. see the locations of the 1938 and the 1874 events in Fig. 13 that are 15 and 25 km apart based on different datasets, respectively). In regions like our study area where the distance between faults is small this can be enough to ascribe seismic events to the wrong fault (*cf.* Fig. 13). A seismic hazard assessment like the one we present here uses fault activity as an input parameter and would, therefore, be wrong in this case. The AUTH catalogue (Papazachos *et al*. 2000) puts the 1938 $M_w = 6.0$ Oropos epicentre into the hangingwall of the Milesi Fault, so that the hypocentre could well fit with this fault. The Makropoulos *et al*. (2012) and UOA catalogues place the epicentre further to the west, away from the Milesi Fault and more than five kilometres into the footwall of another fault (Makropoulos *et al*. 2012). Based on our palaeoseismological analysis we consider it unlikely that the 1938 Oropos earthquake ruptured the Milesi Fault for two reasons: (1) the dating of the palaeosols and the geometry of the hangingwall deformation indicate that the last surface rupturing event occurred after 1800 BP, but no indicators for coseismic movement less than one century ago could be found; (2) postglacial fault scarps developed in the limestone footwall bear kinematic indicators like corrugations, but all scarps show signs of alteration that indicate they have been subjected to erosion for a longer period than only several decades. In fact, the kinematic indicators were weathered to a grade that no precise slip vector could be determined.

None of the major events that are listed in the catalogues except the 1417 event listed by AUTH fits our data, but the 1417 epicentral area is located relatively far to the north of the Milesi Fault (Figs 1 and 13). It must be considered that there is no historical account for the post-1800 BP earthquake that is conserved in the trench. The epicentre of the 1874 event is poorly constrained and it caused only little damage to villages north of our study area. The available catalogues might therefore underestimate the area's seismic activity.

An important finding is that the historical catalogue is not complete for the last 2000 yr—quakes like those that we inferred for the Milesi Fault might go unnoticed, and the magnitude of completeness can be relatively high for events which are older than a few hundreds of years. Important events like the 1705 earthquake have larger errors in their location—the epicentre was somewhere between Athens

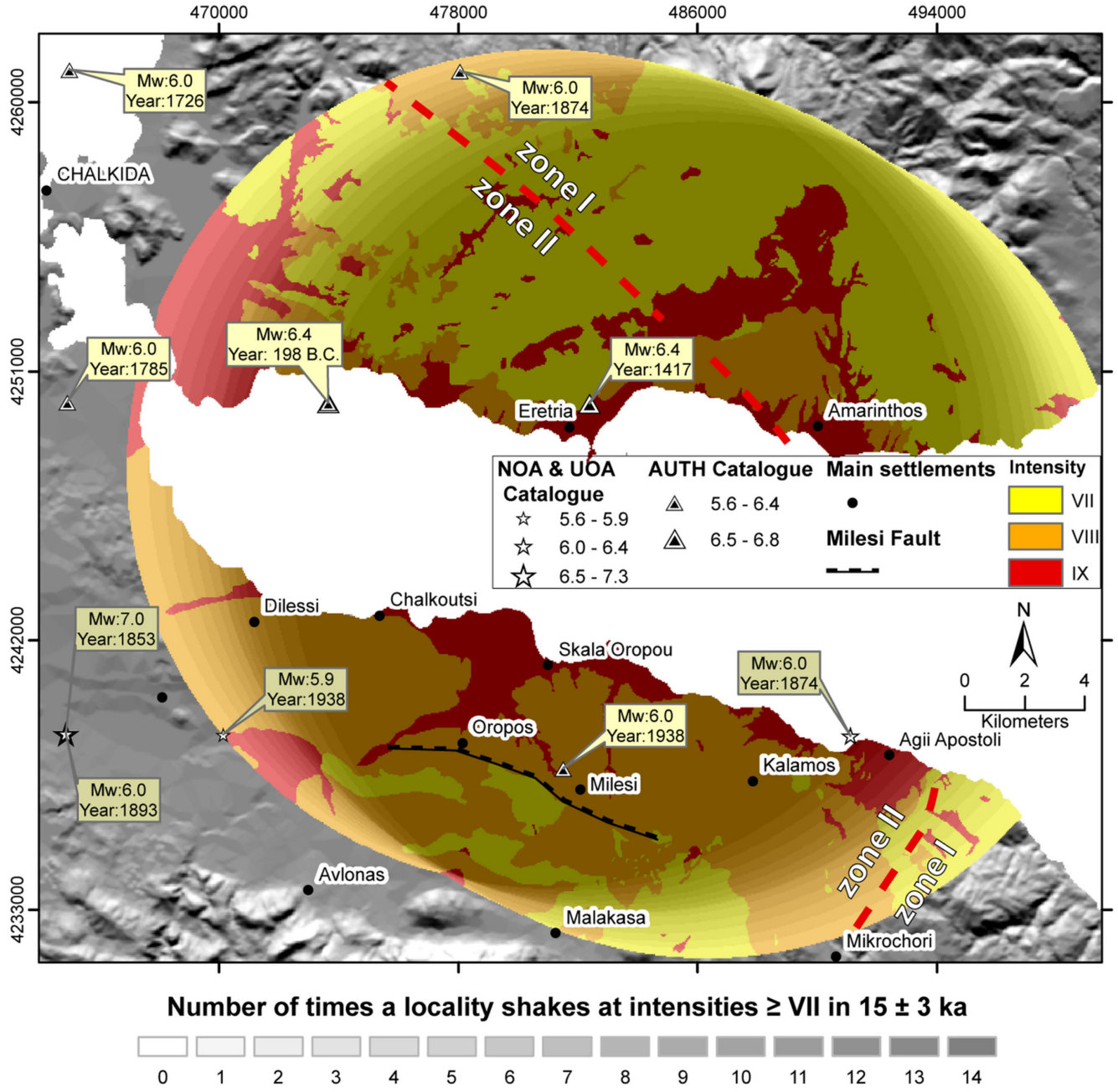

Figure 13. Seismic hazard map showing the maximum expected intensities expected by the activation of the Milesi Fault ranging from intensity VII to IX (MM), after considering the amplification due to the surface geology. Significant damage is expected also on the northern side of the Southern Evoikos Gulf in the island of Evia, where the coastal towns of Eretria and Amarinthos are situated. Historical earthquakes are marked, based on the two catalogues of NOA and UOA (Makropoulos *et al*. 2012) and AUTH (Papazachos *et al*. 2000). Note the differences in the historical data, especially in the location of the 1938 Oropos event, which may easily lead to a misinterpretation of the local fault activity. The latter puts also in question the accuracy of the boundary of the official seismic hazard map that is based on such historical information. The current seismic hazard zonation is indicated with a dashed red line (EAK 2003).

and Chalkida (see Fig. 1). This is a very unsatisfying situation and emphasizes the need for palaeoseismological investigations in the study area. We see that even in areas like Athens, which can be considered to have a relatively good historical record due to a long settlement history with well-known written sources, the available earthquake information is not sufficient to draw conclusions on the tectonic activity of single faults, not to speak from seismic hazard analyses. The more than 2000 yr record of Ambraseys & Psycharis' (2012) 'column seismometer' only tells us that no earthquake was both strong enough and close enough to destroy the monuments, providing limited information on events like the 1999 quake or stronger, but more distant Milesi-type earthquakes.

7.2 Uncertainties in the palaeoseismological analysis

Geomorphological analysis, mapping and palaeoseismological trenching prove that the Milesi Fault is an active tectonic structure. It produced at least four earthquakes with magnitudes ≥ 6 during the last six millennia and created a cumulative vertical offset of about 2 m during that time and of *ca.* 5 m since the last glaciation.

The retrodeformation of the trench log represents the possible scenario. It illustrates an attempt to reconstruct a deformation history as simple as possible. We assumed that all observed downthrow of the palaeosols was created co-seismically and end up with at least four surface rupturing events during the last 6 ka. Another interpretation might be possible (different sedimentation events, additional erosion events, sliding), but we assume that our interpretation is reasonable. However, we cannot rule out the possibility that more earthquakes did occur at the Milesi Fault, which have not ruptured the surface and thus left no traces in the investigated fault zone. Earthquakes with magnitude <5.5 are unlikely to break the surface (e.g. Michetti *et al*. 2000), whereas earthquakes of magnitude $<M_s$ 6 are usually poorly expressed as discontinuous traces or fractures showing inconsistent or no net displacement and are characterised by much shorter surface ruptures than the source length as defined for example by aftershocks (Bonilla *et al*. 1984; Darragh & Bolt 1987; Bonilla 1988).

Taking all these uncertainties into account, we emphasize the most important features of our trench, because even if the retrodeformation can be questioned in details, we can draw some important conclusions. Palaeosol 2 consists of soil material that is found at a depth of up to 1 m, mainly 0.5 m below present-day surface. This material was dated to 1.8 ka BP. If this material was formed in-situ, we would observe a downthrow of ∼0.5 m within 1.8 ka, either in one or in more seismic events. Note that there is no vertical offset at our trench site, the slope surface is smooth. If the material found in P2 was formed further uphill it would then have filled a void that was created by a surface rupturing event after the material was formed. Still, we see ∼0.5 m downthrow within 1.8 ka, that is, the fault moved on average 0.28 mm a^{-1}.

Palaeosol 1 is a thin, distinct layer of organic material at a depth of ∼1.8 m below surface in its southern part and up to 3 m below surface in its northern part, after it kinked. We have three dates from this layer: ∼6, ∼5 and ∼4 ka BP. P1 likely does not represent a real palaeosol layer, but instead material eroded from the slope above our trench and was later affected by ongoing soil forming processes. The different ages then represent different source areas. Therefore, the deposition of the material must have taken place at or after ∼4 ka BP. This means that we see a total of 1.8 m downthrow within not more than ∼4 ka or on average, 0.45 mm a^{-1}. Even if we take into account 0.2 m of recent soil development on top, we end up with 1.6 m in 4 ka, or 0.4 mm a^{-1}.

The length of the Milesi Fault makes it unlikely that single earthquakes produce offsets larger than 1 m and it is likely that not more than a few tens of centimetres of slip can be observed at the surface. In all cases we can reconstruct that a number of earthquakes, possibly four, have downthrown a max. 4-ka-old layer for at least 1.6 m. We can exclude creep as we do not see any sedimentological evidence for this. These findings are strong evidence that the Milesi Fault is active, and they allow us to estimate a throw rate covering at least four events. This rate is consistent with what we see in the Holocene scarp heights, in the geological cross section, in the geomorphology, and what other researchers (e.g. Ganas *et al*. 2005) reconstruct for neighbouring, similar faults. Although the distribution of surface offsets in single earthquakes is known to be highly variable, there are a number of studies which showed that in similar settings (Mediterranean, normal faulting, limestone footwall, soft rock hangingwall, moderate earthquakes of ∼*M*6–*M*7) post glacial scarps do often record series of surface rupturing earthquakes with similar slip or throw characteristics (Benedetti *et al*. 2002, 2003; Bubeck *et al*. 2015; Wiatr *et al*. 2015). This in turn means that the slip that is visible in palaeoseismological trenches at such sites can be used to estimate slip rates, too. Palaeoseismoloical studies performed in Greece support this (e.g. Chatzipetros *et al*. 2005). We wish to emphasize that caution is needed when estimating a throw rate based on trenching, but a combination of different methods like in our study can help to overcome these uncertainties.

The throw rates derived from the retrodeformation are slightly higher than those calculated based on scarp profiling and geological mapping: up to ∼0.45 mm a^{-1} compared to 0.33 ± 0.07 mm a^{-1}. Both values are slightly higher than those previously reported in the literature for some neighbouring normal faults (Ganas *et al*. 2005; Papanikolaou & Papanikolaou 2007). We regard the Milesi throw rate derived from the retrodeformation as a good estimate because: (1) This is the first study to directly measure the throw rate from coseismic offsets; (2) The rates derived from scarp profiling are minimum values since the visible scarp height can have been reduced by erosion and sedimentation in the hangingwall; (3) The value is within the error bars of the other methods and (4) The value would better explain the deformation rates calculated from GPS data, see next section.

We assumed a Holocene age (last glacial maximum at 15 ± 3 ka BP) for calculating throw rates from the scarp heights. This is a generally accepted hypothesis (e.g. Benedetti *et al*. 2002; Papanikolaou *et al*. 2005; Caputo *et al*. 2006) which has a major influence on our calculations. A younger age of the scarps would lead to higher slip rates; an older age would lower our values. We cannot see any geological mechanism that would lead to a younger age of the scarps. The limestones in which the scarps are preserved are massive and not easily to be eroded (Fig. 5) within few thousands of years. A preservation of the scarps during the LGM could be considered, and indeed Hoffmann (2013) found hints for pre-LGM scarps in the Lake Ohrid area in FYROM/Albania. We cannot rule out such effects in our case, but the fact that geomorphological data, palaeoseismological trenching and geodetic data all result in similar slip rates encourages us to assume that our assumption is valid.

7.3 Implications for extensional tectonics in N Attica

The extensional tectonic setting of N Attica led to the development of several E–W trending normal faults west of the Attica Detachment. GPS observations imply that the area is characterized by a strain rate of about 30–50 nstrain a^{-1} (Hollenstein *et al*. 2008; Chousianitis *et al*. 2013; Müller *et al*. 2013) with the maximum horizontal extension in N(NE)–S(SW) direction. The set of normal faults west of the Attica Detachment stretches over a distance of ∼35 km (NE–SW) from the Evoikos Gulf in the north to beyond the Penteli mountain in the south. This means that an extension ∼1.1–1.75 mm a^{-1} would be accommodated by six parallel faults in N Attica, assuming that the deformation occurs on faults that separate rigid blocks and assuming that all deformation is elastic and accommodated by faulting. With a maximum throw rate of ∼0.45 mm a^{-1} for the Milesi Fault, a horizontal slip component of the same amount can be expected for this fault (with a dip angle of 45° at depth). The other faults are longer, but their slip rates are thought to not exceed 0.3 mm a^{-1} (Ganas *et al*. 2005; Papanikolaou & Papanikolaou 2007), resulting in a horizontal extension of not more than 0.17 mm a^{-1}, respectively. Overall, the six faults would accommodate a maximum of ∼1.1 mm a^{-1} of horizontal extension, which is the lowermost bound of deformation expected from GPS measurements. Since the Milesi Fault is the only fault for which primary data on Holocene slip rate is now available, it is likely that the slip rates of the other faults are underestimated, if we assume that

the GPS velocities are correct and reflect geological slip rates. If at least some of the other faults moved slightly faster than currently thought, the GPS rates can be entirely explained by the mapped faults. This would in turn mean that no anelastic strain occurs in this region.

Goldsworthy & Jackson (2001) observed that in active fault systems comprising a set of subparallel normal faults the seismic activity over time migrates towards the faults in the basin centres, accommodating the majority of the overall strain. They studied the Northern Evoikos Gulf and the Gulf of Corinth among others using geodetic motion data, geomorphological observations and historical earthquakes. In the Southern Evoikos Gulf, the Holocene earthquake history of the Milesi Fault testifies that recent motion also occurs away from the coastal fault and other offshore faults known in this graben. Our observations indicate that the 1938 earthquake unlikely occurred on the Milesi Fault, while seismicity is not restricted to the basin centre here. Other faults in the area being situated further inland show signs of recent activity like morphological evidence and Holocene fault scarps (Ganas *et al*. 2005; Papanikolaou & Papanikolaou 2007).

The observations of Goldsworthy & Jackson (2001) can, however, explain the misfit between crustal deformation rates derived from GPS and from our study: If the faults in the basin centre (Southern Evoikos Gulf) accommodate most of the present day motion, then the coastal fault could slip much faster than the ones onshore and make up for the deficit in horizontal strain. This would in return mean that these had either shorter earthquake recurrence intervals or associated magnitudes greater than expected. Since the fault north of the Milesi Fault is longer (possibly up to 40 km), this hypothesis is likely. The seismic hazard posed by the coastal fault would in either case be significantly higher than the one caused by the Milesi Fault.

There is a clear difference between the maximum magnitudes calculated from the visible offsets in the trench (up to *M*6.5 following Ambraseys & Jackson 1998) and those calculated from fault length mapping (up to *M*6.3). A possible explanation would be that the length of the Milesi Fault is underestimated. We mapped a 9.7 km long fault trace with clear surface expressions. The western termination of the fault is formed by a gentle decrease in morphological expression, which does not allow an unambiguous determination of the end of the fault on this side. The eastern tip of the fault diminishes in a mountainous area, which also complicates to pinpoint an end. The Milesi Fault might in fact be a bit longer due to these uncertainties. The empirical relationships used for magnitude estimation like the ones of Wells & Coppersmith (1994) in general perform somewhat better for large earthquakes than for smaller ones. One reason for this is the phenomenon of shallow slip deficit, that is, not all the slip that occurs at depth reaches the surface. It is difficult to account for this uncertainty in palaeoseismological investigations and it is one of the main sources of error, which in many cases prohibits the assessment of palaeomagnitudes. Maximum slip per event seems to scale linearly with fault length (e.g. Scholz 1982) and is commonly accepted to be in the order of $1–6 \times 10^5$ the fault length. For the 9.7 km long Milesi Fault a slip of ∼1 m at depth can be expected, which would also indicate possible earthquakes of $\sim M_w$ 6.3.

7.4 Implications for seismic hazard

The recurrence interval of surface rupturing events of magnitude ≥6 at the Milesi Fault is 1000–1500 a based on the presented results. Our estimates show that intensities up to IX must be expected in some parts of the study area, namely close to the fault and in sedimentary basins (Fig. 13). Locations on bedrock are far less likely to experience such strong shaking, but intensity VII will occur, too (Fig. 13). The Milesi Fault does not pose a significant threat to Athens itself based on this scenario. The model, however, illustrates that strong ground motion must be expected also on the northern side of the Evoikos Gulf. Intensity IX is calculated for the cities of Eretria and Amarinthos. This result questions the validity of the official seismic hazard zonation that is based on historical data, as the boundary between seismic zones I and II crosses the island of Evia and the two municipalities belong to different zones (Figs 1 and 13). From a geological point of view this is not justifiable. It must be considered that faults like the one north of the Milesi Fault could lead to even higher intensities if they rupture along their entire length.

Recently, several studies have shown that earthquakes of magnitude 6–6.5 in a similar tectonic setting are likely to cause significant earthquake environmental effects (EEEs) such as liquefaction, landslides, lateral spread and rockfalls (Michetti *et al*. 2007; Papanikolaou *et al*. 2009; Fountoulis & Mavroulis 2013; Mavroulis *et al*. 2013; Pavlides *et al*. 2013). With intensity IX lateral spread is likely to affect also the coastal areas of our study area, including the port of Oropos from which a ferry connects Attica with Evia. Liquefaction has previously been observed here, for example during the 1938 event (Ambraseys & Jackson 1990; Papathanassiou *et al*. 2005). Papathanassiou *et al*. (2010) report that other parts of our study area are also susceptible to liquefaction, in particular coastal flats where intensity IX is expected. Close to the Milesi Fault, steep limestone cliffs and scarps could also pose an additional rockfall hazard, as suggested by the boulders found in the trench. Landslides could be triggered in the relatively soft Neogene sediments that are present in the coastal area of northern Attica. However, this will depend on the timing of a future quake. Landslides are much more likely to occur in winter than in summer since most of the precipitation occurs in winter months and the water content of the sediments strongly controls cohesion and the internal friction angle.

8 CONCLUSIONS

This study shows that the Milesi Fault is an active structure affecting northern Attica. We conducted geomorphological analyses, field mapping and palaeoseismological trenching in order to determine the slip rate of the fault. Our data reveal that the slip rate of the Milesi Fault is higher than previously suggested, namely 0.2–0.45 mm a^{-1}. The lower values are based on scarp height mapping, the higher values are derived from the retrodeformation of the trench log.

We identified at least four palaeoearthquakes that happened on this fault during the last 4–6 ka. Maximum magnitudes are 6.2–6.5. The average recurrence interval at the Milesi Fault is 1000–1500 a. With these input values we run a fault specific seismic hazard assessment. The scenario shows that the official seismic hazard zonation in our study area likely underestimates the hazard posed by the Milesi Fault. Furthermore, the seismic zonation is not justified by geological fault data. A comparison of available historic earthquake data with geological information makes clear that instrumental seismicity and historical sources are not sufficient to assess the seismic hazard correctly in areas where the average recurrence interval of seismic events is rather large and where faults move slowly.

We found hints that the 1938 Oropos earthquake did not occur on the Milesi Fault. Our data suggest that the slip rates of the set of subparallel faults that characterizes the study area are likely to be underestimated in the literature. In contrast to the Northern Evoikos Gulf and other parts of Greece undergoing extension, fault activity seems not to be confined to the faults in the centre of the Southern Evoikos Gulf graben system. Instead, a significant amount of extension is accommodated by structures closer to Athens.

ACKNOWLEDGEMENTS

Michael Arvanitis from GSSI greatly supported our field work with geophysical equipment. We thank Dimitrios Papanikolaou, Angela Landgraf, Petra Štěpančíková, James Jackson and Alex Copley for helpful discussions on an earlier version of the manuscript. Anonymous reviewers provided very useful comments that helped to improve the paper. Some figures were prepared with the Generic Mapping Tools (GMT) software by Wessel & Smith (1998).

REFERENCES

AHEAD Working Group, 2014. *The European Archive of Historical Earthquake Data,* AHEAD, doi:10.6092/INGV.IT-AHEAD, Available at: http://www.emidius.eu/AHEAD/main/, last accessed 19 April 2014.

Ambraseys, N.N. & Jackson, J.A., 1990. Seismicity and associated strain of central Greece between 1890 and 1988, *Geophys. J. Int.,* **101,** 663–708.

Ambraseys, N.N. & Jackson, J.A., 1997. Seismicity and strain in the Gulf of Corinth (Greece) since 1694, *J. Earthq. Eng.,* **1,** 663–708.

Ambraseys, N.N. & Jackson, J.A., 1998. Faulting associated with historical and recent earthquakes in the Eastern Mediterranean region, *Geophys. J. Int.,* **133**(2), 390–406.

Ambraseys, N.N. & Psycharis, I.N., 2012. Assessment of the long-term seismicity of Athens from two classical columns, *Bull. Earthq. Eng.,* **10,** 1635–1666.

Avramidou, E., Papaioannou, P. & Deloukas, A., 2009. Summer holidays and seasonal travel activities in Attica: a panel-based comparative approach, in *Proceedings of the European Transport Conference,* Leiden, The Netherlands, 5–7 October.

Benedetti, L., Finkel, R., Papanastassiou, D., King, G., Armijo, R., Ryerson, F., Farber, D. & Flerit, F., 2002. Post-glacial slip history of the Sparta fault (Greece) determined by ^{36}Cl cosmogenic dating: evidence for non-periodic earthquakes, *Geophys. Res. Lett.,* **29**(8), doi:10.1029/2001GL014510.

Benedetti, L. *et al.*, 2003. Motion on the Kaparelli fault (Greece) prior to the 1981 earthquake sequence determined from ^{36}Cl cosmogenic dating, *Terra Nova,* **15**(2), 118–124.

Boncio, P., Lavecchia, G. & Pace, B., 2004. Defining a model of 3D seismogenic sources for seismic hazard assessment applications: the case of central Apennines (Italy), *J. Seismol.,* **8**(3), 407–425.

Bonilla, M.G., 1988. Minimum earthquake magnitude associated with coseismic surface faulting, *Bull. Assoc. Eng. Geologists,* **25,** 17–29.

Bonilla, M.G., Mark, R.K. & Lienkaemper, J.J., 1984. Statistical relations among earthquake magnitude, surface rupture length, and surface fault displacement, *Bull. seism. Soc. Am.,* **68,** 411–428.

Bradley, K., 2012. The roof of the Cyclades: a structural, stratigraphic, and paleomagnetic investigation of neogene extension in Central Greece, *PhD thesis,* Massachusetts Institute of Technology, 302 pp.

Bradley, K.E., Vassilakis, E., Hosa, A. & Weiss, B.P., 2013. Segmentation of the Hellenides recorded by Pliocene initiation of clockwise block rotation in Central Greece, *Earth planet. Sci. Lett.,* **362,** 6–19.

Bronk Ramsey, C., 2009. Bayesian analysis of radiocarbon dates, *Radiocarbon,* **51**(1), 337–360.

Bubeck, A., Wilkinson, M., Roberts, G.P., Cowie, P.A., McCaffrey, K.J.W., Phillips, R. & Sammonds, P., 2015. The tectonic geomorphology of bedrock scarps on active normal faults in the Italian Apennines mapped using combined ground penetrating radar and terrestrial laser scanning, *Geomorphology,* **237,** 38–51.

Caputo, R., 2005. Ground effects of large morphogenic earthquakes, *J. Geodyn,* **40**(2), 113–118.

Caputo, R. & Pavlides, S., 2013. Greek Database of Seismogenic Sources (GreDaSS), doi:10.15160/unife/gredass/0200, last accessed 7 August 2015.

Caputo, R., Monaco, C. & Tortorici, L., 2006. Multiseismic cycle deformation rates from Holocene normal fault scarps on Crete (Greece), *Terra Nova,* **18**(3), 181–190.

Caputo, R., Mucciarelli, M. & Pavlides, S., 2008. Magnitude distribution of linear morphogenic earthquakes in the Mediterranean region: insights from palaeoseismological and historical data, *Geophys. J. Int.,* **174**(3), 930–940.

Chatzipetros, A., Kokkalas, S., Pavlides, S. & Koukouvelas, I., 2005. Palaeoseismic data and their implication for active deformation in Greece, *J. Geodyn,* **40,** 170–188.

Chen, W.P. & Molnar, P., 1983. Focal depths of intracontinental and intraplate earthquakes and their implications for the thermal and mechanical properties of the lithosphere, *J. geophys. Res.,* **88**(B5), 4183–4214.

Chousianitis, K., Ganas, A. & Gianniou, M., 2013. Kinematic interpretation of present-day crustal deformation in central Greece from continuous GPS measurements, *J. Geodyn.,* **71,** 1–13.

Darragh, R.B. & Bolt, B.A., 1987. A comment on the statistical regression relation between earthquake magnitude and fault rupture length, *Bull. seism. Soc. Am.,* **77,** 1479–1484.

Degg, M., 1992. Natural disasters: recent trends and future prospects, *Geography,* **77**(3), 198–209.

Doblas, M., 1998. Slickenside kinematic indicators, *Tectonophysics,* **295,** 187–197.

Drakatos, G., Karastathis, V., Makris, J., Papoulia, J. & Stavrakakis, G., 2005. 3D crustal structure in the neotectonic basin of the Gulf of Saronikos (Greece), *Tectonophysics,* **400,** 55–65.

EAK, 2003. Greek Seismic Zonation, *Official Governmental Gazette,* 1154, Athens, August 2003 (in Greek).

Ekström, G., Nettles, M. & Dziewonski, A.M., 2012. The global CMT project 2004–2010: centroid-moment tensors for 13 017 earthquakes, *Phys. Earth planet. Inter.,* **200–201,** 1–9.

Foumelis, M., Fountoulis, I., Papanikolaou, I. & Papanikolaou, D., 2013. Geodetic evidence for passive control of a major Miocene tectonic boundary on the contemporary deformation field of Athens (Greece), *Ann. Geophys.,* **56**(6), S0674.

Fountoulis, I.G. & Mavroulis, S.D., 2013. Application of the Environmental Seismic Intensity scale (ESI 2007) and the European Macroseismic Scale (EMS-98) to the Kalamata (SW Peloponnese, Greece) earthquake (Ms = 6.2, September 13, 1986) and correlation with neotectonic structures and active faults, *Ann. Geophys.,* **56**(6), S0675.

Ganas, A., Pavlides, S.B., Sboras, S., Valkaniotis, S., Papaioannou, S., Alexandris, G.A., Plessa, A. & Papadopoulos, G.A., 2004. Active fault geometry and kinematics in Parnitha Mountain, Attica, Greece, *J. Struct. Geol.,* **26,** 2103–2118.

Ganas, A., Pavlides, S. & Karastathis, V., 2005. DEM-based morphometry of range-front escarpments in Attica, central Greece, and its relation to fault slip rates, *Geomorphology,* **65,** 301–319.

Goldsworthy, M. & Jackson, J., 2001. Migration of activity within normal fault systems: examples from the Quaternary of mainland Greece, *J. Struct. Geol.,* **23**(2), 489–506.

Goldsworthy, M., Jackson, J. & Haines, J., 2002. The continuity of active fault systems in Greece, *Geophys. J. Int.,* **148,** 596–618.

Grützner, C., Barba, S., Papanikolaou, I. & Pérez-López, R., 2013. Earthquake geology: science, society and critical facilities, *Ann. Geophys.,* **56**(6), S0683.

Hamblin, W.K., 1976. Patterns of displacement along the Wasatch fault, *Geology,* **4**(10), 619–622.

Hoffmann, N., 2013. The active tectonic landscape of Lake Ohrid (FYR of Macedonia/Albania), *Ann. Geophys.,* **56**(6), S0678, doi:10.4401/ag-6254.

Hollenstein, C., Müller, M.D., Geiger, A. & Kahle, H.-G., 2008. Crustal motion and deformation in Greece from a decade of GPS measurements, 1993–2003, *Tectonophysics,* **449,** 17–40.

Jackson, J.A. & White, N.J., 1989. Normal faulting in the upper continental crust: observations from regions of active extensions, *J. Struct. Geol.,* **11**(1/2), 15–36.

Jacobshagen, V., 1986. *Geologie von Griechenland,* Vol. 19, Gebrüder Borntraeger.

Jolivet, L. *et al.*, 2013. Aegean tectonics: strain localisation, slab tearing and trench retreat, *Tectonophysics,* **597,** 1–33.

Katsikatsos, G., 2000. *1:50 000 Geological Map Sheet Eretria,* Institute of Geology and Mineral Exploration (IGME).

Kontoes, C., Elias, P., Sykioti, O., Briole, P., Remy, D., Sachpazi, M., Veis, G. & Kotsis, I., 2000. Displacement field and fault model for the September 7, 1999 Athens earthquake inferred from ERS2 satellite radar interferometry, *Geophys. Res. Lett.,* **27**(24), 3989–3992.

Kouskouna, V. & Makropoulos, K., 2004. Historical earthquake investigations in Greece, *Ann. Geophys.,* **47**(2–3), 723–731.

Krohe, A., Mposkos, E., Diamantopoulos, A. & Kaouras, G., 2010. Formation of basins and mountain ranges in Attica (Greece): the role of Miocene to recent low-angle normal detachment faults, *Earth-Sci. Rev.,* **98,** 81–104.

Makropoulos, K., Kaviris, G. & Kouskouna, V., 2012. An updated and extended earthquake catalogue for Greece and adjacent areas since 1900, *Nat. Hazards Earth Syst. Sci.,* **12,** 1425–1430.

Mavroulis, S.D., Fountoulis, I.G., Skourtsos, E.N., Lekkas, E.L. & Papanikolaou, I.D., 2013. Seismic intensity assignments for the 2008 Andravida (NW Peloponnese, Greece) strike-slip event (June 8, Mw = 6.4) based on the application of the Environmental Seismic Intensity scale (ESI 2007) and the European Macroseismic Scale (EMS-98), *Ann. Geophys.,* **56**(6), S0681.

McCalpin, J.P., 2009. Chapter 3: Paleoseismology in extensional tectonic environments, in *Paleoseismology,* pp. 171–269, Elsevier (International Geophysics).

McKenzie, D., 1978. Active tectonics of the Alpine—Himalayan belt: the Aegean Sea and surrounding regions, *Geophys. J. Int.,* **55**(1), 217–254.

Michetti, A.M., Ferreli, L., Esposito, E., Porfido, S., Blumetti, A.-M., Vittori, E., Serva, L. & Roberts, G.P., 2000. Ground effects during the 9 September 1998, M_w = 5.6, Lauria earthquake and the seismic potential of the "Aseismic" Pollino region in Southern Italy, *Seism. Res. Lett.,* **71,** 31–46.

Michetti, A.M., Audemard, F.A. & Marco, S., 2005. Future trends in paleoseismology: integrated study of the seismic landscape as a vital tool in seismic hazard analyses, *Tectonophysics,* **408**(1), 3–21.

Michetti, A.M. *et al.*, 2007. Intensity scale ESI 2007, in *Memorie Descrittive Carta Geologica d'Italia,* Vol. 74, 53 pp., eds Guerrieri, L. & Vittori, E., APAT, Servizio Geologico d'Italia— Dipartimento Difesa del Suolo.

Mouzakis, H.P., Psycharis, I.N., Papastamatiou, D.Y., Carydis, P.G., Papantonopoulos, C. & Zambas, C., 2002. Experimental investigation of the earthquake response of a model of a marble classical column, *Earthquake Eng. Struc. Dyn.,* **31**(9), 1681–1698.

Müller, M.D., Geiger, A., Kahle, H.-G., Veis, G., Billiris, H., Paradissis, D. & Felekis, S., 2013. Velocity and deformation fields in the North Aegean domain, Greece, and implications for fault kinematics, derived from GPS data 1993–2009, *Tectonophysics,* **597–598,** 34–49.

NOA, 2014. Geodynamic Institute of the National Observatory of Athens, Moment Tensor Catalogue, Available at: http://bbnet.gein.noa.gr/, last accessed 18 August 2014.

Pace, B., Peruzza, L. & Visini, F., 2010. LASSCI2009. 2: layered earthquake rupture forecast model for central Italy, submitted to the CSEP project, *Ann. Geophys.,* **53**(3), 85–97.

Pantosti, D., Collier, R., D'Addezio, G., Masana, E. & Sakellariou, D., 1996. Direct geological evidence for prior earthquakes on the 1981 Corinth fault (central Greece), *Geophys. Res. Lett.,* **23**(25), 3795–3798.

Papadimitriou, E.E. & Karakostas, V.G., 2003. Episodic occurrence of strong ($M_w \geq 6.2$) earthquakes in Thessalia area (central Greece), *Earth planet. Sci. Lett.,* **215,** 395–409.

Papadopoulos, G.A., Drakatos, G., Papanastassiou, D., Kalogeras, I. & Stavrakakis, G., 2000a. Preliminary results about the catastrophic earthquake of 7 September 1999 in Athens, Greece, *Seismol. Res. Lett.,* **71**(3), 318–329.

Papadopoulos, G.A., Vassilopoulou, A. & Plessa, A., 2000b. *A Catalogue of Historical Earthquakes for Central Greece: 480 B.C.–1910 A.D.,* Institute of Geodynamics, National Observatory of Athens, Publ. No. 11.

Papanikolaou, I.D., 2003. Generation of high resolution seismic hazard maps through integration of earthquake geology, fault mechanics theory and GIS techniques in extensional tectonic settings, *Unpublished PhD thesis,* University of London, 437 pp.

Papanikolaou, D., 2009. Timing of tectonic emplacement of the ophiolites and terrane paleogeography in the Hellenides, *Lithos,* **108,** 262–280.

Papanikolaou, D. & Lozios, S., 1990. Comparative neotectonic structure of high (Korinthia-Beotia) and low rate (Attica-Cyclades) activity (in Greek), *Bull. Geol. Soc. Greece,* **26,** 47–66.

Papanikolaou, D.I. & Papanikolaou, I.D., 2007. Geological, geomorphological and tectonic structure of NE Attica and seismic hazard implications for the northern edge of the Athens plain, *Bull. Geol. Soc. Greece,* **40,** 425–438.

Papanikolaou, D.J. & Royden, L.H., 2007. Disruption of the Hellenic arc: late Miocene extensional detachment faults and steep Pliocene-Quaternary normal faults—Or what happened at Corinth?, *Tectonics,* **26**(5), 1–16.

Papanikolaou, D.I., Mariolakos, E.L. & Lekkas, E.L., 1988a. Morphotectonic observations on the Assopos basin and the coastal zone of Oropos. Contribution to the Neotectonics of Northern Attica, *Bull. Geol. Soc. Greece,* **20,** 251–267 (in Greek).

Papanikolaou, D., Lykousis, V., Chronis, G. & Pavlakis, P., 1988b. A comparative study of neotectonic basins across the Hellenic arc: the Messiniakos, Argolikos, Saronikos and Southern Evoikos Gulfs, *Basin Res.,* **1,** 167–176.

Papanikolaou, D., Chronis, G., Likousis, V. & Pavlakis, P., with the contribution of Roussakis, G. & Syskakis, D., 1989. *Submarine Neotectonic Map of Southern Evoikos Gulf, 1:100 000,* E.P.P.O., March 1989.

Papanikolaou, I.D., Roberts, G.P. & Michetti, A.M., 2005. Fault scarps and deformation rates in Lazio-Abruzzo, Central Italy: comparison between geological fault slip-rate and GPS data, *Tectonophysics,* **408,** 147–176.

Papanikolaou, I.D., Papanikolaou, D.I. & Lekkas, E.L., 2008. Low slip-rate faults around big cities: a challenging threat. The Afindai fault as a case study for the city of Athens, in *Proceedings of the 14th World Conference on Earthquake Engineering,* 2008 October 12–17, Beijing, China, pp. 1–8.

Papanikolaou, I.D., Papanikolaou, D.I. & Lekkas, E.L., 2009. Advances and limitations of the environmental seismic intensity scale (ESI 2007) regarding near-field and far-field effects from recent earthquakes in Greece: implications for the seismic hazard assessment, *Geol. Soc., Lond., Spec. Publ.,* **316**(1), 11–30.

Papanikolaou, I.D., Roberts, G.P., Deligiannakis, G., Sakellariou, A. & Vassilakis, E., 2013. The Sparta Fault, Southern Greece: from segmentation and tectonic geomorphology to seismic hazard mapping and time dependent probabilities, *Tectonophysics,* **597,** 85–105.

Papantonopoulos, C., Psycharis, I.N., Papastamatiou, D.Y., Lemos, J.V. & Mouzakis, H.P., 2002. Numerical prediction of the earthquake response of classical columns using the distinct element method, *Earthq. Eng. Struct. Dyn.,* **31**(9), 1699–1717.

Papathanassiou, G., Pavlides, S., Christaras, B. & Pitilakis, K., 2005. Liquefaction case histories and empirical relations of earthquake magnitude versus distance from the broader Aegean region, *J. Geodyn,* **40**(2), 257–278.

Papathanassiou, G., Valkaniotis, S., Chaztipetros, A. & Pavlides, S., 2010. Liquefaction susceptibility map of Greece, in *Bulletin of the Geological Society of Greece, Proceedings of the 12th International Congress,* Patras, May 2010, pp. 1–10.

Papazachos, B.C., 1990. Seismicity of the Aegean and surrounding area, *Tectonophysics,* **178,** 287–308.

Papazachos, B.C. & Papazachou, C.B., 1997. *The Earthquakes of Greece,* Ziti Editions, Thessaloniki, 304 pp.

Papazachos, B., Comninakis, P., Karakaisis, G., Karakostas, B., Papaioannou, Ch., Papazachos, C. & Skordilis, E., 2000. A catalogue of earthquakes in Greece and surrounding area for the period 550BC-1999,

Publ. Geoph. Lab., Univ. of Thessaloniki, Available at: http://geophysics.geo.auth.gr/ss/CATALOGS/seiscat.dat, last accessed 30 June 2014.

Pavlides, S. & Caputo, R., 2004. Magnitude versus faults' surface parameters: quantitative relationships from the Aegean Region, *Tectonophysics,* **380**(3), 159–188.

Pavlides, S.B., Papadopoulos, G. & Ganas, A., 2002. The fault that caused the Athens September 1999 Ms = 5.9 Earthquake: field observations, *Nat. Hazards,* **27,** 61–84.

Pavlides, S., Papathanassiou, G., Valkaniotis, S., Chatzipetros, A., Sboras, S. & Caputo, R., 2013. Rock-falls and liquefaction related phenomena triggered by the June 8, 2008, $M_w = 6.4$ earthquake in NW Peloponnesus, Greece, *Ann. Geophys.,* **56**(6), S0682.

Perissoratis, C. & van Andel, T.H., 1991. Sea-level changes and tectonics in the Quaternary extensional basin of the South Evvoikos Gulf, Greece, *Terra Nova,* **3**(3), 294–302.

Psycharis, I.N., 2007. A probe into the seismic history of Athens, Greece from the current state of a classical monument, *Earthquake Spect*., **23,** 393–415.

Psycharis, I.N., Lemos, J.V., Papastamatiou, D.Y., Zambas, C. & Papantonopoulos, C., 2003. Numerical study of the seismic behaviour of a part of the Parthenon Pronaos, *Earthq. Eng. Struc. Dyn.,* **32**(13), 2063–2084.

Reimer, P.J. *et al.*, 2013. IntCal13 and Marine13 radiocarbon age calibration curves 0–50 000 years cal BP, *Radiocarbon,* **55**(4), 1869–1887.

Reiter, L., 1990. *Earthquake Hazard Analysis: Issues and Insights,* Columbia Univ. Press, 254 pp.

Roberts, G.P., Cowie, P., Papanikolaou, I. & Michetti, A.M., 2004. Fault scaling relationships, deformation rates and seismic hazards: an example from the Lazio-Abruzzo Apennines, central Italy, *J. Struct. Geol.,* **26,** 377–398.

Rondoyanni, T., Galanakis, D., Georgiou, C. & Baskoutas, I., 2007. Identifying fault activity in the central Evoikos Gulf (Greece), *Bull. Geol. Soc. Greece,* **40,** 439–450.

Scholz, C.H., 1982. Scaling laws for large earthquakes: consequences for physical models, *Bull. seism. Soc. Am.,* **72**(1), 1–14.

Scholz, C.H., Aviles, C.A. & Wesnousky, S.G., 1986. Scaling differences between large interplate and intraplate earthquakes, *Bull. seism. Soc. Am.,* **76,** 65–70.

SHARE Project, 2014. Seismic Hazard Harmonization in Europe. Project of the seventh framework programme of the European Commission, Available at: http://www.share-eu.org.

Smith, A.D., 1994. Late Quaternary tectonics, sedimentation and sea-level changes in the north Aegean region, *PhD thesis,* University of Cambridge, Cambridge, p. 202.

Stewart, I. & Hancock, P., 1988. Normal fault zone evolution and fault scarp degradation in the Aegean region, *Basin Res.,* **1**(3), 139–153.

Stiros, S.C., 1995. Archaeological evidence of antiseismic constructions in antiquity, *Ann. Geophy.,* **38**(5–6), 725–736.

Stiros, S.C. & Pirazzoli, P.A., 1995. Palaeoseismic studies in Greece: a review, *Quater. Int.,* **25,** 57–63.

Taymaz, T., Jackson, J. & McKenzie, D., 1991. Active tectonics of the north and central Aegean Sea, *Geophys. J. Int.,* **106**(2), 433–490.

Theodulidis, N.P., 1991. Contribution to strong ground motion study in Greece, *PhD Thessaloniki,* University of Thessaloniki.

Theodulidis, N.P. & Papazachos, B.C., 1992. Dependence of strong ground motion on magnitude-distance, site geology and macroseismic intensity for shallow earthquakes in Greece: I. Peak horizontal acceleration, velocity and displacement, *Soil Dyn. Earthq Eng.,* **11,** 387–402.

Vayas, I., Dasiou, M.-E. & Marinelli, A., 2007. Saeulen griechischer Tempel unter Erdbebenbeanspru-chung, *Bautechnik,* **84**(6), 388–396 (in German).

Wells, D.L. & Coppersmith, K.J., 1994. New empirical relationships among magnitude, rupture length, rupture width, rupture area, and surface displacement, *Bull. seism. Soc. Am.,* **84**(4), 974–1002.

Wessel, P. & Smith, W.H., 1998. New improved version of Generic Mapping Tools released, *EOS, Trans. Am. geophys. Un.,* **79**(47), 579.

WGCEP, 2002. Working Group on California Earthquake Probabilities. Earthquake probabilities in the San Francisco Bay region: 2002–2013, USGS Circular 1189.

Wiatr, T., Papanikolaou, I., Fernández-Steeger, T. & Reicherter, K., 2015. Bedrock fault scarp history: insight from t-LiDAR backscatter behaviour and analysis of structure changes, *Geomorphology,* **228,** 421–431.

Zygouri, V., Koukouvelas, I.K., Kokkalas, S., Xypolias, P. & Papadopoulos, G.A., 2013. The Nisi Fault as a key structure for understanding the active deformation of the NW Peloponnese, Greece, *Geomorphology,* **237,** 142–156.